1
The MALDI Process and Method

Franz Hillenkamp, Thorsten W. Jaskolla, and Michael Karas

1.1
Introduction

Matrix-assisted laser desorption/ionization (MALDI) is one of the two "soft" ionization techniques besides electrospray ionization (ESI) which allow for the sensitive detection of large, nonvolatile and labile molecules by mass spectrometry. Over the past 27 years, MALDI has developed into an indispensable tool in analytical chemistry, and in analytical biochemistry in particular. In this chapter, the reader will be introduced to the technology as it stands now, and some of the underlying physical and chemical mechanisms as far as they have been investigated and clarified to date will be discussed.

Attention will also be focused on the central issues of MALDI, that are necessary for the user to understand for the efficient application of this technique. As an in-depth discussion of these topics is beyond the scope of this chapter, the reader is referred to recent reviews [1–4]. Details of the current state of instrumentation, including lasers and their coupling to mass spectrometers, will be presented in Chapter 2.

As with most new technologies, MALDI came as rather a surprise even to the experts in the field on the one hand, but also evolved from a diversity of prior art and knowledge on the other hand. The original notion had been that (bio)molecules with masses in excess of about 500–1000 Da could not be isolated out of their natural (e.g., aqueous) environment, and even less be charged for an analysis in the vacuum of a mass spectrometer without excessive and unspecific fragmentation. During the late 1960s, however, Beckey introduced *field desorption* (FD), the first technique to open a small road into the territory of *mass spectrometry* (MS) of bioorganic molecules [5]. Next came *secondary ion mass spectrometry* (SIMS), and in particular static SIMS, as introduced by A. Benninghoven in 1975 [6]. This development was taken a step further by M. Barber in 1981, with the bombardment of organic compounds dissolved in glycerol with high-energy atoms, which Barber coined *fast atom bombardment* (FAB). It was in this context, and in conjunction with the first attempts to desorb organic molecules with laser irradiation, that the concept of a "matrix" as a means of facilitating desorption and enhancing ion

MALDI MS: A Practical Guide to Instrumentation, Methods, and Applications, Second Edition.
Edited by Franz Hillenkamp and Jasna Peter-Katalinic.

yield was born [7]. The principle of desorption by the bombardment of organic samples with the fission products of the ^{252}Cf nuclear decay, later termed *plasma desorption* (PD), was first described by R. Macfarlane in 1974 [8]. Subsequently, the groups of Sundqvist and Roepstoff greatly improved the analytical potential of this technique by the addition of nitrocellulose, which not only cleaned up the sample but was also suspected of functioning as a signal-enhancing matrix [9].

The first attempts at using laser radiation to generate ions for a mass spectrometric analysis were reported only a few years after the invention of the laser [10, 11]. Vastola and Pirone had already demonstrated the possibility of recording the spectra of organic compounds with a *time-of-flight* (TOF) mass spectrometer. Subsequently, several groups continued to pursue this line of research, mainly R. Cotter at Johns Hopkins University in the USA and P. Kistemaker at the FOM Institute in Amsterdam, the Netherlands. Indeed, for a number of years the Amsterdam group held the high-mass record for a bioorganic analyte with a spectrum of underivatized digitonin at mass 1251 Da ($[M + Na]^+$), desorbed with a CO_2-laser at a wavelength of 10.6 µm in the far infrared (IR) [12].

Independently of, and parallel to, these groups, Hillenkamp and Kaufmann developed the *laser microprobe mass analyzer* (LAMMA) [13], the commercial version of which was marketed by Leybold Heraeus in Cologne, Germany and which is now on exhibition in the section on New Technologies of the Deutsches Museum in Munich, Germany. The instrument originally comprised a frequency-doubled ruby laser at a wavelength of 347 nm in the near ultraviolet (UV), and later a frequency-quadrupled Nd:YAG-laser at a wavelength of 266 nm in the far UV. The laser beam was focused to a spot of ≤1 µm in diameter to probe thin tissue sections for inorganic ions and trace elements such as Na, K, and Fe. The mass analyzer of the LAMMA instruments was also a TOF mass spectrometer, and was the first commercial instrument with an ion reflector, which had been invented a few years earlier by B.A. Mamyrin in Leningrad. The sensitivity-limiting "noise" of the LAMMA spectra were signals that were soon identified as coming from the organic polymer used to embed the tissue sections, as well as other organic tissue constituents. It was this background noise which triggered the search for a systematic analysis of organic samples and which eventually led to the discovery of the MALDI principle in 1984. The principle and its acronym were first described in 1985 [14], and the first spectrum of the nonvolatile bee venom mellitin, an oligopeptide at mass 2845 Da, in 1986 [15]. Spectra of proteins with masses exceeding 10 kDa and 100 kDa were reported in 1988 [16], and details presented at the International Mass Spectrometry Conference in Bordeaux in 1988, respectively.

Both, ESI and MALDI were developed independently but concurrently, and when their potential for the desorption of nonvolatile, fragile (bio)molecules was discovered, the scientific community was mostly impressed by the ability of these techniques to access the high mass range, particularly of proteins. However, FAB- and PD-MS had at that time already generated spectra of trypsin at mass 23 kDa and other high-mass proteins. What really made the difference in particular for the biologists was the stunning sensitivity which, for the first time, made

MS compatible with sample preparation techniques used in these fields. For MALDI, the minimum amount of protein needed for a spectrum of high quality was reduced from 1 pmol in 1988 to a few femtomoles only about a year later. Today, in favorable cases, the level is now down in the low attomole range. Many other developments – both instrumental (see Chapter 2) as well as specific sample preparation recipes and assays (see other chapters of the book) – took place during the following decade, and the joint impact of all of these together has today made MALDI-MS an indispensable tool not only in the life sciences but also in polymer analysis, food sciences, pharmaceutical drug discovery, or forensic jurisprudence.

The use of a chemical matrix in the form of small, laser-absorbing organic molecules in large excess over the analyte is at the core of the MALDI principle. Several developments for laser desorption schemes took place in parallel to and following publications of the MALDI principle. These all attempted to replace the chemical matrix by a more easy-to-handle physical matrix, or a more simple combination of the two. The best known of these was the system of Tanaka and coworkers, which was first presented at a Sino-Japanese conference in 1987; the details were subsequently published in 1988 [17]. The matrix comprised cobalt-nanoparticles suspended in glycerol as the basic system into which the analyte was dissolved, similar to the sample preparation of FAB. Several other nano- and micro-particles were tested later, and results obtained that were comparable to those of Tanaka [18]. For his technique of *surface-assisted laser desorption/ionization* (SALDI), Sunner and coworkers used dry carbon and graphite substrates [19]. Another technique which has attracted much interest for the analysis of smaller molecules (and which is described in more detail in Chapter 9) was reported by Siuzdak [20]. This method, termed *desorption/ionization on silicon* (DIOS), uses preparations of neat organic samples on porous silicon. Several other methods and acronyms use similar systems, such as nanowires or sol–gel systems. All of these methods use the substrate on which the analyte is prepared for the absorption of the laser energy, and are characterized by a sensitivity which is lower than that of MALDI by several orders of magnitude, as well as a strongly increased ion fragmentation which limits the accessible mass range to somewhere between 2000 and 30 000 Da, depending on the method. There is reason to believe that all of these methods are based on a thermal desorption at the substrate/analyte interface, with the high internal excitation of the ions and low ion yield typical for thermal desorption processes. The very high heating and cooling rates, together with high peak temperatures of the substrates as well as the suspension of the absorbers in glycerol, apparently soften the desorption somewhat, the latter most probably through adiabatic cooling in the expanding plume; derivatization of the surfaces can up-concentrate the analyte of interest at the surfaces to increase the sensitivity. Indeed, a yoctomole (10^{-21} mole) sensitivity has been achieved in this way with a perfluorophenyl-derivatized DIOS system for a small hydrophobic peptide [21].

Recently, another technique termed *matrix-assisted inlet ionization* (MAII) was described by Trimpin *et al.*, which enables the generation of multiply charged

analyte ions similarly to those observed with ESI [22]. Although the analytes to ionize are also cocrystallized with typical MALDI matrices, the energy required for material ablation can be supplied by laser irradiation (*laserspray ionization* with laser pulse energies of about 10-fold that typically used for MALDI MS [22]), but is not limited to it [23]. It is assumed that analyte ion generation occurs independently of, and subsequent to, the ablation process in a heated inlet tube connecting the atmospheric pressure source to the vacuum of the mass spectrometer. Until now, the process of charge generation has not been completely understood; however, matrix evaporation of ablated highly charged clusters/droplets within the heated tube seems to explain the generation of multiply charged analytes. Due to the aforementioned differences to common MALDI MS, this technique is not discussed in this book.

1.2 Analyte Incorporation

What, then, is so special about the chemical matrix in MALDI? Some of its important features, such as the absorption of the laser energy, are easily understood, but rather surprisingly the overall process of the desorption and ionization has not yet been fully described, almost 30 years after its invention. Considerable progress regarding the mechanism of analyte desorption and protonation was recently achieved [24, 25]. Meanwhile, the search for better (i.e., more sensitive) matrices does not remain completely empirical, as some of the critical parameters for efficient analyte protonation (see Section 1.5) are uncovered, although other aspects such as prediction and targeted manipulation of the matrix morphology remain [26].

One important feature is the way in which the matrix and analyte interact in the MALDI sample. In a typical UV-MALDI "dried droplet" sample preparation, small volumes of an about 10^{-6}–10^{-9} M solution of the analyte and a near-saturated (ca. 0.01–0.1 M) solution of the matrix are mixed; the solvent is then evaporated before the sample is introduced into the vacuum of the mass spectrometer. Upon solvent evaporation, the matrix crystallizes in a specific morphology to form a bed of small crystals that range in size from a few to a few hundred micrometers, depending on the matrix, the solvent, the substrate surface characteristics, and further details of the preparation. The typical molar analyte-to-matrix ratio ranges from about 10^{-2} for less-sensitive compounds such as poorly protonable drugs without basic functionalities, to approximately 10^{-7} for highly sensitive analytes, for example, quaternary ammonium-derivatives such as phosphatidylcholines or many basic peptides. The sample preparation is discussed in more detail in Section 1.8. One of the early surprises in MALDI development was that all of the well-functioning matrices known at that time incorporated the analytes in the crystals quantitatively (up to a maximum concentration), and in a homogeneous (on the light microscopic resolution level of 0.5 μm) distribution. This was shown for the UV-MALDI matrices 2,5-dihydroxybenzoic acid (2,5-DHB) [27], sinapic acid [28], α-cyano-4-

hydroxycinnamic acid (HCCA) [29], and 3-hydroxypicolinic acid [29] as well as the IR-MALDI matrix succinic acid [30]. This homogeneous incorporation, in conjunction with the also homogeneous energy deposition and material ablation (for a discussion, see Section 1.3) resulted in the codesorption of intact nonvolatile and labile molecules with the matrix and, in addition, in a cooling of their internal energy in the expanding plume of material. Although the mechanisms and driving force for analyte incorporation are still largely unknown, attractive ion–ion interactions between dissolved protonated analytes and matrix acid anions during sample preparation seem to alleviate analyte inclusion/incorporation within the growing matrix crystals [26]. At typically slightly acidic sample preparation conditions, many analytes (such as most peptides and proteins) carry net positive charges due to protonated basic and predominantly neutralized acidic functionalities. Although matrix acid functionalities are also mostly neutralized under such pH conditions, the large molar matrix-to-analyte excess effects matrix anion amounts sufficiently high for at least stoichiometric analyte interactions in solution. These ion–ion interactions might provide the explanation of why almost all compounds used as matrices for the analysis of basic group containing analytes – which is the case for many natural drug classes – exhibit acid functionalities. Neutral α-cyanocinnamic acid (CCA) derivatives, for example, matrix amides or esters with weaker ion–dipole interactions between protonated analytes and neutral matrices, indeed resulted in strongly diminished analyte signal intensities.

Nevertheless, further prerequisites for successful analyte inclusion/incorporation presumably must be fulfilled. Krueger *et al*. found clear proof for homogeneous analyte incorporation by using colored pH indicators [31], whereas Horneffer *et al*. have shown in a systematic study of different position isomers of dihydroxybenzoic acids that only 2,5-DHB incorporates homogeneously and quantitatively, whereas other isomers such as 2,6-DHB do not incorporate at all, while some others incorporate only randomly [32]. Confocal laser scanning images of the protein avidin, labeled with the fluorochrome Texas Red for single crystals of 2,5-DHB and 2,6-DHB, are shown in Figure 1.1. No obvious correlation between analyte incorporation and the crystal structure of these isomers was found.

The state of the incorporated analyte molecules in the matrix crystals is another interesting question. Based on results obtained for the incorporation of pH-indicator dye molecules, Krueger *et al*. have concluded that molecules retain their solution charge state in the crystal, which implies that they also retain their solvation shell [31]. Horneffer *et al*. have found a high density of cavities of 10–2000 nm size in crystals of both 2,5-DHB and 2,6-DHB by electron microscopy [33]. At first sight, these cavities could be assumed to contain analyte molecules with residual solvent. However, if this is the case it is difficult to understand why 2,5-DHB – but not 2,6-DHB – incorporates analytes into these cavities; attempts to localize gold-labeled proteins in the cavities of 2,5-DHB were also inconclusive [33].

A solventless method for sample preparation was developed originally for the MALDI-MS of synthetic polymers, which often are not soluble in standard solvents [34]. In this method, matrix and analyte powders are mixed and ground in a mortar

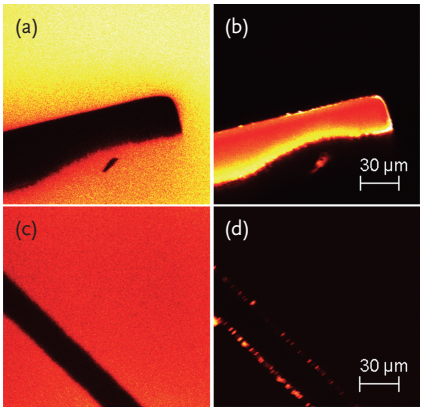

Figure 1.1 Confocal laser scan fluorescence images of single crystals of (a, b) 2,5-dihydroxybenzoic acid and (c, d) 2,6-dihydroxybenzoic acid. Both matrices were doped with the protein avidin, labeled with a Texas Red fluorescent dye. The images were recorded at a x,y-plane 12 µm into the crystals. Panels (a) and (c) show dark shadowgraphs of the shape of the crystals against the bright green BODIPY 493/503 fluorescence of the immersion liquid (false color photography). Panels (b) and (d) show the red Texas Red fluorescence of the labeled proteins.

or ball-mill and then applied to a MALDI target support. It was shown that analyte spectra can be obtained from such preparations, even though the analyte is only chemisorbed at the matrix crystal surfaces [35]. However, the desorption is much less "soft" than MALDI-MS from samples with incorporated analytes, leading to a strongly increased metastable fragmentation of the ions and an upper mass limit for proteins of 30–55 kDa.

1.3 Absorption of the Laser Radiation

The role of the optical absorption of the matrix in the transfer of energy from the laser beam to the sample is governed by Beer's law [14]

$$H = H_0 * e^{-\alpha z} \tag{1.1}$$

where H is the laser fluence at depth z into the sample, H_0 is the laser fluence at the sample surface, and α is the absorption coefficient (see Chapter 2, Section 2.2 for a definition of the fluence). The absorption coefficient α equals the product of the wavelength-dependent molar absorption coefficient α_n which is a property of the matrix compound and the concentration c_n of the absorbing molecules in the sample. The molar absorption coefficient α_n has a maximum value for UV-MALDI irradiation of typical matrices between 5×10^3 and 5×10^4 l mol^{-1} cm^{-1} at the peak absorption wavelength. Molar absorption coefficients of this order of magnitude and at low wavelengths in the range of 300–400 nm are only pro-

vided by molecules with aromatic systems (typical matrix structures for instance contain phenyl or styryl derivatives) supported by electron-donating groups such as hydroxy residues. The exact wavelength of maximum absorption and its magnitude are determined by the position and nature of the ligands of the core ring, and are tabulated in a variety of reference sources. Some care should be exercised in using the tabulated values for α_n, because they all refer to dilute solutions of the compounds. Compared to the absorption profiles of dissolved compounds, the absorption bands of MALDI samples in the solid state are typically broadened and slightly red- or blue-shifted in dependence on the strength of the chromophore–solvent interactions of the dissolved compounds [25]. The concentration c_n of absorbers (chromophores) is unusually high in solid-state MALDI samples (about $10\,\mathrm{mol\,l^{-1}}$), taking into account the typical solid-state density of crystals of roughly $2\,\mathrm{g\,cm^{-3}}$ (e.g., 2,3-dihydroxybenzoic acid exhibits a density of $1.54\,\mathrm{g\,cm^{-3}}$), because all of the solvent is evaporated before the sample is introduced into the vacuum. As a result, the typical UV absorption coefficient α ranges from about 5×10^4 to $5 \times 10^5\,\mathrm{cm^{-1}}$ at a laser wavelength of 337 or 355 nm. The inverse of α is called the penetration depth δ, and this has values of only 20 to 200 nm. It is the depth into the sample, at which the fluence has decreased to about 30% of the value at the surface. It is also an order of magnitude estimate of the depth of material ablated (desorbed) per single laser pulse in MALDI. Because of this very shallow ablation depth, a given location of the sample can usually be irradiated many times before the material is exhausted. For the MALDI process, the energy absorbed per unit volume E_a/V of the sample (loosely called "energy density") is the process-determining quantity. This can be derived from Eq. (1.1) by simple differentiation to:

$$E_a/V = \alpha * H \tag{1.2}$$

Equation (1.2) is at the core of the MALDI process. If a matrix is chosen with a sufficiently high absorption coefficient α, a relatively low fluence H_0 suffices for achieving the critical "energy density" necessary to initialize ablation and ionization of a top layer of the sample. Values for H_0 of $50–500\,\mathrm{J\,m^{-2}}$ are representative for most UV-MALDI applications.

As discussed in Chapter 2, Section 2.2, pulsed lasers with a pulse width of a few nanoseconds are employed in UV-MALDI. At a fluence of about $100\,\mathrm{J\,m^{-2}}$ and a pulse width of 2 ns, the "intensity" (irradiance) of the laser beam at the sample surface is only $10^{11}\,\mathrm{W\,m^{-2}}$ or $10^7\,\mathrm{W\,cm^{-2}}$, which is not enough to induce any nonlinear absorption such as nonresonant two-photon absorption. For the linear absorption, the absorbed energy per unit volume can be controlled meticulously with a suitable variable attenuator in the laser beam, a feature which has emerged as being crucial for the successful MALDI of large molecules, because the desorption of nonvolatile, labile molecules can only be achieved in a narrow range of energy "density" between low-energy conditions insufficient for ablation and ionization and high-energy conditions leading to extensive analyte fragmentation (see Section 1.6). The other essential feature of this laser absorption is that the energy is transferred more or less uniformly to a macroscopic sample volume (except for

the attenuation of the fluence into the sample and the fluence profile, as discussed in Chapter 2, Section 2.2). This is very different from the situation in SIMS or PD, where incident particles create minute tracks of atomic dimensions of very high energy density in the sample, with a strong radial decline of energy density. This strongly heterogeneous energy distribution is the main reason for the limitation of these methods for the intact desorption of larger molecules. The fluence can also be converted into a value for the photon flux – that is, the number of photons impinging on the sample per single laser pulse. A typical fluence of $100\,J\,m^{-2}$ [36] corresponds to a photon flux of 1.7×10^{16} photons per cm^2; each carrying an energy of 3.7 eV at the wavelength of 337 nm of the N_2 laser. A molar absorption coefficient of $10^4\,l\,mol^{-1}\,cm^{-1}$ represents a physical absorption cross-section of the chromophore of $1.6 \times 10^{-17}\,cm^2$, resulting in an average of 0.3 photons absorbed per surface matrix molecule (about $110\,kJ\,mol^{-1}$ matrix for 337 nm photons) for any given laser exposure at this fluence. For these considerations, it is assumed that the vast majority of electronic excitation energy is converted into lattice energy by internal conversion (as compared to processes such as fluorescence and chemical reactions). This is a very high density of excitation energy, close to the sum of all noncovalent bond energies of the ablated matrix volume. It is, therefore, not surprising that such a large amount of deposited energy leads to an explosive ablation of the excited sample volume. On the other hand, it renders even resonant two-photon absorption by the matrix rather unlikely. The high density of excited molecules does, however, result in a rather high rate of energy pooling in the sample, in which two neighboring electronically excited molecules pool their energy, with one of them acquiring twice the energy of the first excited singlet state ($S_1, v = 0$) and the other falling back to its ground state [37]. This energy pooling is an important feature in some models for the ionization of the matrix molecules, which requires at least the energy of two photons for an initial photoionization of the matrix molecules [3, 38]. It is elucidated in more detail in Section 1.5.

The situation is similar, but not equal, for IR-MALDI. Optical absorption in the IR region of the spectrum represents a transition between vibrational and/or rotational molecular states. The probabilities for these transitions are typically lower than the electronic transitions in the UV by one to two orders of magnitude. The strongest such transitions are those of the O–H and N–H stretch vibrations near a 3 μm wavelength. The absorption coefficient of water or vacuum-stable ice, but also of the common IR-MALDI matrix glycerol, reaches peak values of $10^4\,cm^{-1}$ in this wavelength region, corresponding to a penetration depth of about 1 μm, which is more than 20-fold that of typical penetration depths in the UV. As a result, the ablated mass per laser exposure in IR-MALDI exceeds that of UV-MALDI by at least a factor of 10, and the sample consumption rate is accordingly higher. Typical laser fluences for IR-MALDI range from 10^3 to $5 \times 10^3\,J\,m^{-2}$. Nonlinear absorption processes are even less likely for such fluences in the IR- as compared to UV-MALDI, and for the photon energy of only 0.4 eV or less even the absorption of several photons by a given chromophore or energy pooling cannot possibly excite single molecules to anywhere near their ionization energy.

1.4 The Ablation/Desorption Process

As discussed above, every laser exposure of a sample leads to the removal of a bulk volume – that is, many monolayers of matrix molecules of the sample. The term "desorption" is, therefore, somewhat ill-chosen for this process, and was so even for the field desorption for which it was originally coined. Ablation (removal of bulk material from surfaces) is the more specific term, and is used interchangeably with desorption throughout this chapter. The processes of material ablation and the ionization of a minor fraction of the matrix and analyte molecules are, no doubt, intimately intertwined, and both take place on a micrometer geometric and a nanosecond time scale. It is experimentally very difficult – if not impossible – to sort out the complex contributions of the physical processes induced by the laser irradiation in all detail. Despite this complexity, it is of considerable merit to treat the ablation and ionization mechanisms separately. From such a discussion, some basic understanding can be derived, particularly, because the vast majority of the ablated material comes off neutral.

Regarding the energy loss out of the excited sample volume during the laser pulse, at least two situations need to be considered which are known as "thermal" and "stress confinement" regimes: Energy dissipation by heat conduction during the laser pulse can be neglected in all cases of UV- as well as IR-MALDI. For a penetration depth of UV-laser radiation of 100 nm, the time constant for heat conduction of typical UV-MALDI matrices is about 10 ns [39] – still a factor of two to three longer than the typical laser pulse width (typically 3 ns for nitrogen lasers and 4–7 ns for Nd:YAG lasers). In the IR, the 10- to 1000-fold smaller absorption coefficients compared to UV matrices [40] causes penetration depths of about 1 μm with corresponding heat conduction time constants of about 1 μs, a factor of about 10 longer than the longest pulse width of lasers (Er:YAG) used in that case. Heat conduction is therefore not important as an energy loss process in MALDI.

The very rapid heating of the sample by the laser radiation resulting from a comparably slow heat conduction is known as a "thermal confinement" regime. This will generate a thermoelastic pressure pulse in the absorbing sample volume which travels out of the excited volume at the speed of sound, carrying away part of the deposited energy. With the speed of sound in typical crystalline matrices of 2000–3000 ms^{-1} and depths of roughly 100 nm in the UV, the acoustic time constant is less than 100 ps, much shorter than the laser pulse width of a few nanoseconds. Even though energy is constantly carried away by the pressure wave, this amounts only to a very small fraction of the total deposited energy. Due to the comparably short transport time for propagation of the pressure pulses out of the irradiated volume by using nanosecond-lasers, the pressure within the excited volume never reaches values high enough to substantially influence the ablation process [39].

For IR-MALDI, the situation can be very different because of the larger penetration depth, resulting in a larger acoustic time constant of about 1 ns. For the desorption with an Er:YAG laser, the pulse width of 100 ns is long compared to

the acoustic time constant, with only a negligible pressure build-up in the excited volume. The pulse width of the optical parametric oscillator (OPO) laser of only 6 ns, however, is on the same order of magnitude as the acoustic time constant, and the system stays close to what is called the "acoustic confinement" or "stress confinement." In this case a very high pressure of several tens of megapascals can build up in the excited volume, which can in turn cause spallation with the generation of microcracks and the ejection of larger bulks of material [40]. Rohlfing *et al.* [41] have investigated the ablation processes by measuring the recoil pressure of the ablated material with a fast acoustic transducer onto which the sample was prepared, while Leisner *et al.* [42] have studied the expanding plume of ablated material with high-speed time-lapse photography, both at a wavelength of 2.94 µm. Both measurements were much easier for IR-MALDI and glycerol as a matrix, because of the greater amount of material ablated. For the short pulse width and near-acoustic confinement, these authors saw pressure pulses of very high amplitude as expected, and time durations comparable to the laser pulse. For the 100-ns pulses of the Er:YAG laser, the pressure amplitude was low, but lasted for several microseconds. The plume photographs revealed that material is removed from the sample for times of up to over 100 µs in both cases. This is certainly somewhat of a surprise, because the TOF analysis had revealed that the ions are only generated during an initial phase of not longer than about 300 ns using glycerol [43].

Similar experiments were conducted by Rohlfing under UV-MALDI conditions [44], using the liquid matrix nitrobenzylalcohol for better sample homogeneity and a desorption wavelength of 266 nm. Expectedly, the recoil pressure was very low – lower even than that of the long-pulse IR-laser – because of the smaller amount of removed material. The recoil pressure pulse lasted for only less than 25 ns, the time resolution of the detection. The plume photographs revealed a material ejection for up to at least several microseconds, again much longer than the ion generation time of at most a few nanoseconds. Some typical plume photographs are shown in Figures 1.2 (IR-irradiation) [42] and 1.3 (UV-irradiation) [44]. The results of these experiments can tentatively be explained by the following models. In IR-MALDI with 100 ns-long Er:YAG-laser pulses, the absorbing volume is superheated to a temperature that is substantially above the boiling temperature due to a slower gas-phase bubble formation and heat diffusion, followed by an explosive volume ejection of material through boiling by heterogeneous nucleation [40]. The situation is similar for UV-MALDI. The longer time course of material ejection in the IR as compared to the UV is caused by a deeper penetration of the radiation into the sample, and a correspondingly higher inertia and residual heat of the excited volume. For the 6-ns pulses in IR-MALDI of the OPO-laser, the ablation process is substantially different. The strong thermoelastic wave is reflected at the sample vacuum interface, thereby reversing its phase. It then travels back into the sample as a tensile wave, transferring the material beyond the liquid spinodal, as described by Vogel and Venugopalan for soft-tissue ablation [45]. Upon this transition, the material goes through a phase explosion by homogeneous nucleation. Even though all of these experiments were conducted on liquid samples to keep reproducibility high, they reflect, most probably, also the

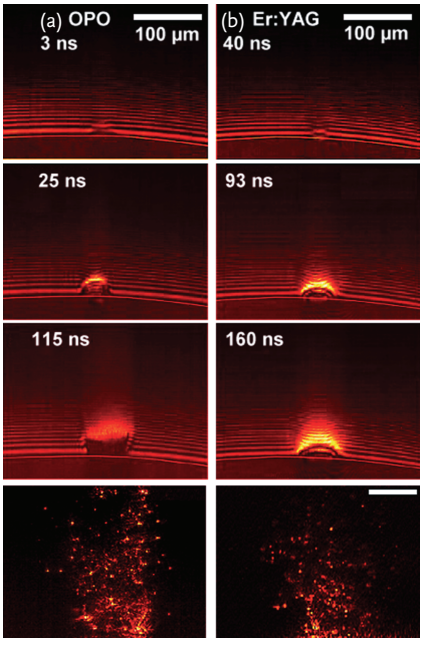

Figure 1.2 High-speed time-lapse photographs of IR-MALDI plumes generated with an optical parametric oscillator laser with 6-ns pulse width (left panels) and an Er:YAG-laser with 100-ns pulse width (right panels). Both lasers were operated at 2.94 µm wavelength. Matrix, glycerol; time resolution, 8 ns; spatial resolution, 4 µm. The top three panels represent gradients of gaseous material density creating gradients of the index of refraction in the plume, recorded in a dark-field illumination mode. The lowest panel represents particle emission in the plume after some µs recorded with light scattered at 90° to the illumination beam. The thin lowest lines indicate the top surface of the glycerol drop; the other striations in the dark-field images are artifacts of optical interference.

situation for crystalline solid samples. A contribution by the gaseous components such as CO_2 through thermal decomposition of matrix molecules as well as *trans–cis*-photoisomerizations of matrices with, for example, cinnamic acid core structures are also discussed as a source of pressure build-up in the excited volume.

Theoretical models for the ionization as well as molecular modeling suggest that the ablation process generates large amounts of (molten) clusters and material particles, besides gaseous components [46]. During the early expansion phase of the plume, dark-field images reveal homogeneous gradients of the index of refraction. However, the spatial resolution of these plume photographs is only a few micrometers; a distribution of clusters of small size, expected during the early phase of the plume expansion, cannot therefore be revealed by this experimental set-up. Nevertheless, nanometer-size particles have indeed been detected by light scattering upon growing the ablated particles by butanol condensation in a cooled tube, although these experiments have been carried out under atmospheric

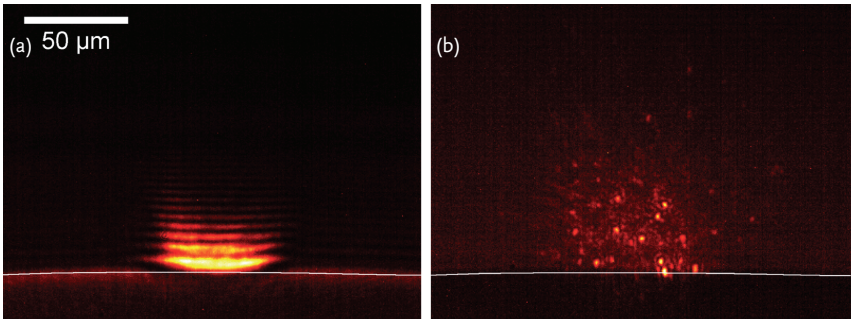

Figure 1.3 High-speed photographic images of UV-MALDI plumes generated with a frequency-quadrupled Nd:YAG laser of 266 nm wavelength and 8 ns pulse width. Matrix, nitrobenzylalcohol; time resolution, 8 ns; spatial resolution, 4 µm. (a) Dark-field image, 45 ns after laser exposure; (b) 90° scattered light image, 311 ns after exposure. The thin lowest line indicates the top surface of the nitrobenzylalcohol drop; the other striations in the dark-field image are artifacts of optical interference.

pressure conditions [47]. In cases when clusters carry net charges they might release analyte ions upon quantitative dissociation (see Section 1.5), provided that sufficient internal thermal cluster energy is available. This energy can derive from chemical intracluster reactions which might be, for example, proton-transfer reactions, fragmentation, dissociation of [2+2]-photodimerized matrices [48], or thermal relaxation of *cis*- to *trans*-isomers after *trans–cis*-photoisomerization. On the other hand, clusters can lose energy by adiabatic expansion in the plume, and the majority of clusters most probably never dissociate completely [49]. In cases of insufficient internal energy, incomplete cluster dissociation of clusters with net charges contributes to the chemical noise/background of mass spectra [49]. Most probably, large clusters (particles) do not contain sufficient internal energy for quantitative dissociation and are stable at least on a nanosecond time scale. This assumption of stable large clusters is further supported by the generation of highly charged analyte ions inside a heated inlet tube attached to the ion source, which is assumed to provide the lacking energy for the complete dissociation of otherwise stable large clusters containing analytes [23], although the parameters used do not correspond with commonly used MALDI conditions. In addition, the origin of the cluster charges generated by this approach remains unclear, since analyte ion generation is not limited to lasers as an energy supply [23]. Consequently, large cluster/particle emission does not seem to be relevant for typical MALDI ion generation.

Garrison, Zhigilei [40, 50] and coworkers, as well as Knochenmuss [38], have modeled the ablation process using molecular dynamics simulations. Qualitatively, these simulations correctly predict many of the features observed experimentally. For example, corresponding to model calculations of Zhigilei and coworkers, mainly single molecules and a small number of dimers and trimers will leave the surface below a threshold fluence. Starting at the threshold fluence

(defined as the minimum energy per irradiated area required for the above-discussed collective ejection process of larger molecular clusters), the intense detection of MALDI ions becomes possible [51]. It must also be observed that these simulations contain significant simplifications and, most probably more restrictive, must be scaled to very small volumes and short time regimes because of limited computation capacity. These models have become significantly refined over the past few years and will, no doubt, continue to do so. In this respect they will clearly contribute to an understanding of MALDI processes in the future.

1.5 Ionization

The mechanisms which lead to the formation of charged matrix and analyte molecules in the MALDI process are even more poorly understood than the physics of the material ablation/desorption. For a better understanding, it is important to distinguish between the ionization of matrix molecules and that of the analytes.

For the standard UV-MALDI laser wavelengths of 337 or 355 nm (i.e., photon energies of 3.7 and 3.5 eV, respectively), more than two photons are needed for the photoionization of a free matrix molecule. However, with increasing matrix aggregate size the ionization potential is lowered somewhat [3, 52] and may come within reach of the sum energy of two photons for the condensed phase. In case a small energy gap has still to be overcome, thermal energy may make up for the difference. The typical MALDI laser photon fluxes are too low for any significant nonresonant and resonant two-photon absorption to take place, but the excited energy of molecules (called excitons) is known to be highly mobile in the crystals with stacked aromatic π-electron systems, such as those of matrices [53]. This allows for the combination of the energy of two excitons with interacting electronic states by which one of the two molecules becomes de-excited to the ground state and the other molecule rises to a higher excited (S_n) state. Very efficient energy pooling between excited matrix molecules in the crystals has indeed been demonstrated at laser fluences typical for MALDI, even though the majority of the absorbed energy becomes converted into lattice energy on a picosecond time scale by internal conversion [37].

Subsequent to photoionization, capture of the released photoelectron by neutral matrix molecules will give rise to complementary negative radical matrix ions beside the positive ions [54]. Due to large cross-sections of dissociated slow electrons, the escape of photoelectrons will be restricted to the very top matrix layers [38]. The frequent observation of radical matrix ions such as $matrix^{+\bullet}$ (Eq. 1.3 [54]) and/or $[matrix + 2H]^{+\bullet}$ and $matrix^{-\bullet}$ (Eq. 1.4 [54]), as well as $[matrix\text{-}2H]^{-\bullet}$ ions, besides the expected even-electron ions, among them $[matrix + H]^+$ – or $[matrix\text{-}H]^-$ – (for assumed formation reactions, see Eqs (1.5) and (1.6) [54]) as well as a prominent $[matrix\ dimer + H\text{-}2H_2O]^+$ for 2,5-DHB and $[matrix\ dimer + H]^+$ for HCCA is at least in agreement with the photoionization model, if not a strong indication for the correctness of this model (Figure 1.4).

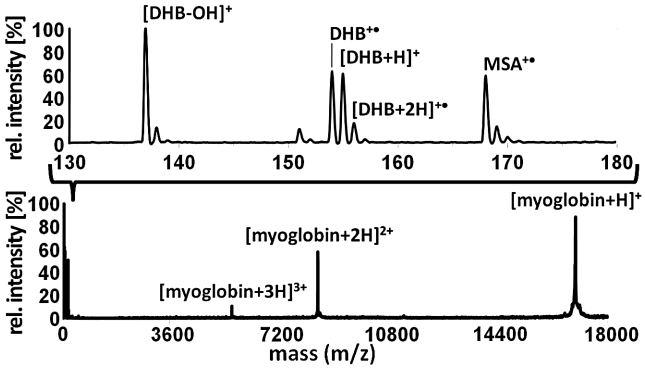

Figure 1.4 UV-MALDI mass spectrum of myoglobin. Matrix: DHBs (2,5-dihydroxybenzoic acid [2,5-DHB] plus 2-hydroxy-5-methoxysalicylic acid [MSA]; 9:1 [w/w]). Wavelength, 337 nm; mass analyzer, reflectron TOF.

$$matrix \xrightarrow{h\nu} matrix^{**} \rightarrow matrix^{+\bullet} + e^{-} \tag{1.3}$$

$$matrix + e^{-} \rightarrow matrix^{-\bullet} \tag{1.4}$$

$$matrix^{+\bullet} + matrix \rightarrow [matrix + H]^{+} + [matrix - H]^{\bullet} \tag{1.5}$$

$$matrix^{-\bullet} + matrix \rightarrow [matrix - H]^{-} + [matrix + H]^{\bullet} \tag{1.6}$$

Although no precise numbers have been determined experimentally, it is, most probably, safe to assume that the ion yield for the matrix (i.e., the ratio of ions to neutrals) which depends on the matrix as well as the laser fluence is somewhere in the range of 10^{-6} to 10^{-4} [55, 56]. The ion yield of the analytes can be much higher, on the order of 0.1–1% for typical compounds, and above 10% in exceptional cases. The intensities of the ion signals, as determined from the spectra, are not independent of each other, because charge-transfer processes from matrix to analyte species as well as among each species are taking place in the expanding plume and possibly already in the solid state upon laser irradiation. In favorable cases, the spectra even show intense analyte ion signals with negligible matrix ions, despite a typical 10^4 excess of the matrix [57]. As the MALDI ionization process starts with the aforementioned matrix ionization, the typically much higher analyte ion yield compared to that of the matrix already indicates a charge transfer and accumulation process in favor of the analyte.

Two models for analyte ion formation have been proposed. The older model – which had not had a well-defined name before 2013 and is now proclaimed as Coupled Physical and Chemical Dynamics (CPCD) model – assumes neutral analyte molecules in the expanding plume – regardless of whether the analytes were incorporated in the matrix crystals as neutral species or were quantitatively neutralized by their counterions upon cluster dissociation in the case of pre-charged incorporated analyte molecules. Subsequent to photoionization of the matrix (Eqs 1.3 and 1.4) and secondary intermolecular matrix reactions leading to the generation of protonated as well as deprotonated matrix ions (Eqs 1.5 and 1.6)

[54], charge transfer to and from the neutral analyte molecules in the plume leads to the generation of [analyte + H]$^+$ Eq. (1.7) and [analyte-H]$^-$ Eq. (1.8).

$$[matrix + H]^+ + analyte \rightarrow matrix + [analyte + H]^+ \tag{1.7}$$

$$[matrix - H]^- (carboxylate) + analyte \leftrightarrow matrix + [analyte - H]^- (carboxylate) \tag{1.8}$$

Knochenmuss has developed a quantitative mathematical model for matrix and analyte ion generation assuming matrix photoionization as the initial step of ion generation. Initially, this was limited to a description of the desorption of individual molecules but, in a later approach, this model was extended to the ejection of a mixture between single molecules and clusters [58].

One argument against photoionization as initial starting point for ion generation is the observation that MALDI spectra, obtained with IR lasers at 1.94 µm wavelength, closely resemble the UV-MALDI spectra, including radical matrix ions observed (e.g., for the succinic acid matrix). The photon energy of only 0.6 eV at this wavelength certainly excludes photoionization. However, similarity of the spectra alone does not suffice as proof of identical ionization processes at the two wavelengths, and indeed the ion yield for analytes in the IR is about an order of magnitude lower than in the UV.

The more recent "lucky survivor" model in its final form assumes that basic analytes, such as most proteins, are incorporated into the matrix as precharged species corresponding to their solution charge state at the point in time they are cocrystallized. This assumption is based on the observation that pH-indicator molecules retain their color and charge state upon crystal incorporation for acidic, neutral, or basic matrices [31]. Furthermore, the addition of extremely strong acids to matrix–analyte preparations led to the gas-phase detection of precharged analyte–acid anion adducts originating from solution [59, 60]. For most common acidic matrices, almost all peptides will carry a (multiple) positive excess charge; counterions will then typically be either matrix or acid (if added to the preparation) anions. For preventing neutralization, the charged peptides must be incorporated in an at least partially solvated form for separation from their counterions by solvent. In a second step, the model assumes a break-up of the crystal lattice into larger and smaller clusters upon desorption, some of them with analyte ions and counterions which will neutralize each other upon cluster dissociation by loss of neutral matrix and possibly remaining solvent molecules. Karas and Krüger assumed that some of these analyte-containing clusters statistically carry one or more excess protonated or deprotonated matrix ions. Upon cluster dissociation, these excess charges are thought to prevent quantitative analyte ion neutralization, leading to the generation of protonated and deprotonated analyte ions [2]. These singly charged analyte ions are the so-called "lucky survivors" of the neutralization process. This model elegantly explains the observation of mostly singly charged ions in MALDI spectra, and works equally well for UV- as well as IR-MALDI. The formation of matrix–analyte clusters in the desorption process is in agreement with experiments in which the ablation of large(r) aggregates was detected under

MALDI-conditions [47] and also predicted by molecular modeling [40, 50]. However, these model calculations also predicted that large clusters would have insufficient internal energy for a complete dissociation with evaporation of the neutrals. This result may also originate from insufficient simulation times and/or to too-limited sizes of the simulation box [58], and does not necessarily reflect the situation for smaller to medium-sized clusters. While the initially charged matrix – analyte cluster ions never appear in the MALDI spectra with the typical solutes used, such as trifluoroacetic acid (TFA) or ammonium salts, they have been detected for extremely strong acids [60]; their conjugate anions are extremely weak bases and thus stabilize the formed ion pairs with protonated analyte sites.

One of the strengths of the lucky-survivor model is that it can be equally well applied to account for the formation of negative ions (if deprotonable groups are present) and positive ions from basic analytes such as peptides and proteins (in solution precharged by protonation; Eqs 1.9 and 1.10), as well as for positive (if protonable groups are present) and negative ions from acidic analytes (in solution precharged by deprotonation; Eqs 1.11 and 1.12) such as nucleic acids:

$$\left\{[analyte + nH]^{n+} + n\,[counterion - H]^- + [matrix + H]^+\right\}^+ \rightarrow [analyte + H]^+ + n\ counterion + matrix \tag{1.9}$$

$$\left\{[analyte + nH]^{n+} + n\,[counterion - H]^- + [matrix - H]^-(carboxylate)\right\}^- \rightarrow \left\{analyte + n\ counterion + [matrix - H]^-(carboxylate)\right\}^- \leftrightarrow [analyte - H]^-(carboxylate) + n\ counterion + matrix \tag{1.10}$$

$$\left\{[analyte - nH]^{n-} + n\,[counterion + H]^+ + [matrix + H]^+\right\}^+ \rightarrow [analyte + H]^+ + n\ counterion + matrix \tag{1.11}$$

$$\left\{[analyte - nH]^{n-} + n\,[counterion + H]^+ + [matrix - H]^-(carboxylate)\right\}^- \rightarrow \{analyte + n\ counterion + [matrix - H]^- - (carboxylate)\}^- - \leftrightarrow [analyte - H]^-(carboxylate) + n\ counterion + matrix \tag{1.12}$$

where {} is a symbol for the intermediate cluster. The commonly observed lower sensitivity of basic analytes (e.g., peptides and proteins) as anions in the negative-ion mode, in contrast to the typically higher detection sensitivities of their corresponding protonated species, is reflected by the CPCD model as well as the lucky survivor. Typical matrix molecules with proton affinities roughly between 800 and 900 kJ mol^{-1} [61], and especially the even more acidic halogenated α-cyanocinnamic acid derivatives recently introduced by Jaskolla *et al.* [26, 62, 63], are in their protonated states strong gas-phase acids in comparison to basic amino acids with much higher proton affinities (up to 1025 kJ mol^{-1} for arginine) [64]. This results in an efficient proton transfer and formation of positively charged analyte ions, as postulated by the CPCD model of Eq. (1.7). The "lucky survivor" model also postulates an efficient generation of protonated basic analytes, as randomly incorporated protonated matrix molecules (resulting from photoionization) in clusters with precharged basic analytes and corresponding counterions lead to a very exo-

thermic counterion neutralization by $[matrix+H]^+$ upon cluster dissociation, which in turn results in the survival of a precharged analyte (Eq. 1.9).

In contrast, no such difference in basicity between the negatively charged ions of matrix molecules and peptides exists, because both are typically carboxylate anions with very close proton affinities. Peptide anion generation competes with simple dissociation of the neutral analyte–matrix anion adduct and limits the yield of analyte anions (see Eq. 1.8 for the CPCD model and Eq. 1.10 for the "lucky survivor").

Similar arguments hold for the polyanionic nucleic acids. While the addition of ammonium ions results in a quantitative detection of the free acids as singly charged cations or anions, substitution of the ammonium ions by tetraalkyl ammonium ions leads to the observation of adduct ions, increasing in intensity with increasing length of the alkyl chains.

Both models – protonation of neutral analytes in the gas phase according to the CPCD model as well as the revised lucky survivor – are discussed in detail in Refs [3, 24, 65].

With the help of deuterated matrices Jaskolla and Karas have recently proven that both models – gas-phase (de)protonation (CPCD model) as well as "lucky survivor" – exist as parts of a greater overall mechanism [24]. These authors concluded that neutral peptides are protonated according to the CPCD model, whereas for slightly basic analytes such as nicotinamide both models contribute to charging. Basic analytes (e.g., peptides) are predominantly protonated by the "lucky survivor," although several factors such as laser fluence, preparation solution pH, analyte size and the difference between matrix and analyte proton affinity may affect or even swap the dominating charging mechanism [24]. The previously detected influence of the matrix proton affinity or, being more precise, the achievable sensitivity increase by use of low-proton affinity matrices [26], is now in excellent agreement with the predictions made by this unified analyte protonation mechanism.

For analytes of very low proton affinity, such as neutral carbohydrates and many synthetic polymers, cationization by Na^+, K^+ or other metal cations is usually observed in MALDI (see Chapters 6–8). The cationization in all likelihood takes place in the expanding plume, and requires a codesorption of the analyte and the cations. Hence, the best results are obtained from sample locations where both species exist in close neighborhood, such as in the center of DHB-dried droplet preparations. Specific protocols have been developed for the MALDI of such analytes [66, 67].

1.6 Fragmentation of MALDI Ions

The fragmentation of MALDI ions is a mixed blessing, as in all of MS. It can, on the one hand, lead to a substantial loss of spectra quality such as loss of mass resolution or even complete loss of the signal of the intact parent ion, as has been

shown for the loss of sialic acids in the analysis of glycoconjugates in reflectron-TOF analyzers [68]. On the other hand, intrinsic or induced fragmentation is an indispensable tool for the acquisition of structural information in MS^n experiments. The nomenclature for the fragmentation – particularly the differentiation in post-source-decay (PSD) and in-source-decay (ISD) ions – is closely related to TOF analyzers, because they still constitute the majority of spectrometers used for the analysis of MALDI ions. The details of how to analyze fragment ions with different types of instrument are discussed in Chapter 2 (see Section 2.4.3 in particular).

Even though some limited ion stability – and thus fragmentation – was obvious in the early days of MALDI by peak tailing on the low mass side, and was attributed to small neutral losses of peptide and protein ions, the fact that MALDI can generate substantial prompt and metastable fragmentation of analyte ions was obscured at an early stage. This was due to two facts: (i) the laser microprobe instrument (LAMMA 1000) used for the initial experiments indeed minimized fragmentation because of a very weak acceleration field strength and a low total (3 keV) ion energy; and (ii) the next-generation of MALDI-TOF instruments were linear instruments in which only less-intense prompt but no metastable fragment ions can be observed directly.

It was only when Kaufmann and Spengler began careful investigations of ion stability using a deceleration stage in a linear TOF instrument that the potentially high degree of metastable fragmentation was detected [69]. This was the starting point for the development of the so-called PSD analysis of metastable ions which has led to today's MALDI-TOF/TOF instruments (the first "TOF" refers to generation and isolation of the precursor ion, and the second "TOF" to separation and identification of the generated fragment ions) [70, 71]. Modern instruments enable faster and better-resolved PSD measurements by ion fragmentation in a collision cell, followed by an increase in the potential energy of the (precursor and fragment) ions and their subsequent separation by means of a post-acceleration cell, for example, by the "LIFT" technology [72] or the TOF/TOF-version by Vestal *et al.* [73]. The character of the PSD fragmentation – that is, the classes of fragment ions observed – is in full agreement with a collisional activation process. Despite this general agreement, PSD mass spectra are often more complex than collisionally induced dissociation (CID) mass spectra, showing internal fragments and products of consecutive fragmentations, and pointing to more complex excitation mechanisms of the intramolecular degrees of freedom. An overview between different MALDI fragmentation processes is available in Refs [74, 75].

Besides collisional excitation through collisions of the analyte ions with neutrals in the plume upon applying an acceleration voltage, absorption of the laser energy by the matrix with subsequent thermal energy transfer to analytes already in the solid state, as well as subsequently in the early phase of the dense plume, are possible causes for fragmentation. In addition to exothermic plume reactions such as electron attachment, the exothermicity of gas-phase proton-transfer reactions is a further widely suggested driving force for analyte fragmentation [76, 77]. The thermal energy (temperature) of analyte ions depends in complex fashion on

instrumental parameters such as laser wavelength, fluence and focus, as well as on the matrix-specific absorption properties [25]. These laser parameters further influence the plume properties with increasing axial velocities at higher laser fluences and laser pulse length-dependent sizes of ablated clusters [58] which, in combination with strength and delay of the ion extraction field, affects the collisional activation.

Information about the different contributions to ion excitation has been listed in a report which compares vacuum MALDI to atmospheric-pressure (AP)-MALDI. These results were obtained by well-understood correlations between the extent of unimolecular fragmentation of substituted benzylpyridinium ions and their internal ion energy [78]. A comprehensive summary of the current knowledge of MALDI fragmentation is available in Refs [78–80]. The effect of collisional excitation upon prompt acceleration was demonstrated for matrix ions. These AP-MALDI investigations were later extended to determine initial MALDI plume excitation processes [81], including the application to more representative test samples than thermometer molecules, such as model peptides and deoxynucleosides. Schulz *et al.* detected a rough correlation between the extent of fragmentation and the exothermicity of gas-phase analyte protonations by protonated matrices: the lower the matrix proton affinity (PA) and higher the analyte gas-phase basicity, the more internal analyte energy was available for fragmentation [81]. Similar conclusions were drawn by Stevenson *et al.*, when investigating analyte deprotonation reactions. With increasing gas-phase basicities of the investigated deprotonated matrix anions, more internal energy was released upon analyte deprotonation, leading to a more intense analyte fragmentation [76]. In contrast, a recent analysis concluded that the energy released upon exothermic gas-phase reactions would be insufficient for analyte fragmentation [82]. In agreement with this, 4-chloro-α-cyanocinnamic acid (ClCCA) is much softer than HCCA [83], even though it has a clearly lower PA [26]. This points to the existence of additional parameters influencing the matrix "hard-/softness" (causing intense or low analyte fragmentation, respectively). In additional experiments, it was found that the matrix "softness" roughly correlated with the initial ion velocities determined in a linear TOF. In some – but not all – cases, "hard" matrices correlated with low initial velocities [76, 81, 84]. Indeed, ClCCA was seen to exhibit an initial velocity that somewhat exceeded that of HCCA [84], although it was unclear if this increase would fully explain the detected differences in fragmentation. In addition to the assumption that the exothermicity of gas-phase reactions is the most important parameter, additional parameters such as expansion cooling in the MALDI desorption process might further influence the matrix "hard-/softness."

In a practical approach, matrices are classified and ranked from "hard" to "soft." For example, HCCA – the matrix which is preferentially applied for "peptide-mass fingerprint" analyses in proteomics because of its rather homogeneous sample morphology and relatively high sensitivity – is one of the "hardest" matrices in that ranking. Because of its degree of fragmentation induction, it is also the matrix of choice for PSD- or TOF/TOF-experiments. "Super DHB" (DHBs; 2,5-DHB with a 5–10% addition of 2-hydroxy-5-methoxybenzoic acid), 6-aza-2-thiothymine

(ATT), and especially 3-hydroxypicolinic acid (3-HPA) [81], are on the "soft" end of the list and are therefore preferentially applied for the analysis of larger proteins. By using such a "soft" matrix and optimizing all instrumental parameters (low extraction field strength and long extraction delay times for improved resolution and lower plume densities resulting in less collisions and collisional activation upon ion acceleration), small-neutral loss can be minimized and a good mass resolution (close to the theoretical limit) is obtainable for a linear TOF configuration, even for medium-sized proteins up to bovine serum albumin [85]. Alternative matrices for the MALDI-MS analysis of high-molecular-weight compounds comprise ionic liquids [86] (see Section 1.8.3). Common to PSD and the low-energy CID mechanisms is the randomization of the internal energy among all internal degrees of freedom with (metastable) fragmentation preferentially of the most labile bonds [87].

A very different fragmentation mechanism was first reported by R.S. Brown *et al.* [88, 89], whereby fragment ions are formed "promptly" upon ion generation/excitation with a time delay of ≤100 ns, which is substantially less than the typical delay times in delayed-extraction TOF instruments. Therefore, these are referred to as in-source-decay (ISD) ions. The ISD spectra of proteins contain signals of c- and sometimes z-type fragment ions, in addition to some a-, b-, and y-ions [90, 91] (for fragment ion nomenclature, see Chapter 3), but is not limited to peptides and proteins and can also be used for the sequencing of, for example, oligonucleotides such as DNA or RNA [92] or carbohydrates [93, 94]. This type of fragmentation is observed for both positive and negative ions [90], indicating that ISD is independent of proton transfer. Initially, 2,5-DHB was the matrix of choice for high ISD yields [90, 95]; nevertheless, upon the introduction of a method for quantifying matrix ISD-efficiencies [96] it was mainly replaced by more reactive compounds such as 5-aminosalicylic acid (5-ASA) [97] or 1,5-diaminonaphthalene (1,5-DAN), which exhibit very efficient radical transfer abilities to analytes [96, 98]. However, the latter matrix is carcinogenic and generates strong, potentially interfering matrix cluster ion peaks up to about 1000 Da [77]. More recent developments have included nontoxic and highly efficient ISD matrices, for example, 2-aminobenzamide and 2-aminobenzoic acid [91]. The similarity of ISD spectra to those of electron capture dissociation prompted an initial discussion on the possible role of electrons in ISD, but it is clear today that ISD is mediated by hydrogen radicals [95, 99], as was demonstrated by the in-source reduction of disulfide bonds [100]. In the positive-ion mode this includes hydrogen abstraction from matrix molecules to peptides, followed by a unimolecular fragmentation of the peptide radical or a cleavage upon collision with a second matrix molecule [101]. Unfortunately, the nomenclature of ISD and PSD relates to the specific source geometry of linear TOF instruments rather than to the two different fragmentation processes. This has led to some confusion as to which process is causing which fragment [80, 82].

Although ISD yields substantially more complete fragment-ion series as compared to PSD, previous intentions to use ISD for practical applications (e.g., in proteomics [102, 103]) have not yet fully materialized. This is due mostly to the

low intensity of the fragment ion signals, which only recently has been considerably improved by the introduction of the aforementioned higher reactive matrices [104, 105]. An additional problem is that true MS/MS experiments cannot be carried out in linear TOF instruments, as a precursor selection for peptides from a mixture is not possible. This leads to complex fragment spectra with overlapping ion signals deriving from multiple fragmented precursor species if no previous precursor separation (e.g., LC-MS/MS) was performed.

1.7 MALDI of Noncovalent Complexes

After about 25 years' use of MALDI-MS, it is clear that the successful analysis of noncovalent interactions and complexes is the exception rather than the rule. Yet, when considering most typical MALDI protocols, this cannot be a surprise. Most "classical" matrices are organic acids and typically are used in water/organic solvent mixtures, often acidified by formic acid (FA) or TFA – that is, under conditions which should result in the dissociation of most (if not all) noncovalent complexes. However, signals of noncovalent complexes have indeed been obtained from such preparations [106, 107]. At least for some such systems, the dissociation seems to be sufficiently slow that a rapid evaporation of the solvent conserves at least a certain fraction of the complexes. Unfortunately, adjustment of the pH and the omission of organic solvent is often not a viable alternative, as acidic matrices will be deprotonated and totally change their crystallization and incorporation properties as salts. Many of the salts and buffers that are used to adjust ionic strength/pH are, therefore, not MALDI-compatible in the desired concentrations, or at least they compromise performance with respect to sensitivity and mass resolution. Nevertheless, the use of sinapic acid with a higher water solubility allows for the preparation of purely aqueous matrix solutions. In combination with a physiological pH, at which sinapic acid still crystallizes as a neutral species, noncovalent protein complexes were retained during sample preparation and could consistently be detected using MALDI [108].

The incorporation of analytes into the matrix crystals, which as such has been shown to make the desorption process softer or altogether possible [35], is another step that might lead to dissociation of the complexes. This question has been addressed in order to understand the so-called "first-shot phenomenon," which had been observed much earlier but was resolved only recently [109, 110]. For a number of selected matrices, the signals of protein–protein complexes are observed only in the spectra of first exposures of a given sample spot. Subsequent exposures yield only signals of the monomer units. However, by employing a combination of MALDI-MS and confocal laser scanning microscopy (CLSM) of noncovalent complexes with fluorochromes, which exhibit a fluorescence resonance energy transfer (FRET), it could be shown that in these systems the complexes would dissociate upon incorporation, whereas intact complexes would precipitate at the surface of the matrix crystals. The next crucial step is the intact desorption and

ionization of the complexes, and their survival in the gas phase of the expanding plume. Such dissociation upon desorption is even more likely if the complexes are localized at the crystal surface rather than being incorporated.

The type of interaction within the complex is also a decisive parameter. From energetic considerations it is clear that the stability of noncovalent complexes is highest for ionic interactions, followed by ion–dipole forces and hydrogen bonding. Interestingly, the formation of strong ionic complexes has even been used to facilitate MALDI measurements of highly acidic (and thus negatively charged) biocompounds, such as DNA, oligonucleotides and heparin-derived oligosaccharides. This was achieved by admixing highly basic peptides (e.g., histones), followed by a mass determination of the intact stable complex in the positive-ion mode [111]. Hydrophobic interactions were shown to be particularly labile and to result in a predominant gas-phase dissociation of complexes bound largely by such forces [112].

This effect can be explained by a loss of the hydrophilic environment of polar solvents in the liquid state upon transfer into the vacuum. The facile detection of noncovalent complexes by ESI shows, that the transfer of noncovalent complexes into the vacuum does not necessarily result in dissociation, if the internal energy does not suffice for intermolecular bond-breaking and transition to the very different conformational monomeric states. It would also appear that large contact areas between the constituents of the complex and the corresponding contributions of salt- and hydrogen bridges, as well as hydrophobic interactions typical of many protein–protein complexes, help to stabilize the complex. Consequently, complexes including small molecules, as are typical for ligand–receptor and antigen–antibody systems or specific channel-forming antibiotics, are much more difficult to analyze when using MALDI-MS. Their affinities depend on the exact conservation of the conformation in small epitopes of the protein, which is more easily lost in the MALDI process than is the complete quaternary structure. Interestingly, spectra of the intact biotin–streptavidin complex, which has a dissociation constant of 10^{-15} M and is one of the strongest complexes known to date, have never been obtained by MALDI.

Another issue which complicates the use of MALDI for the analysis of noncovalent complexes is the formation of nonspecific multimeric and adduct ions. This effect is even more pronounced for the analysis of noncovalent protein complexes, as high concentrations (10 pmol μl^{-1} or higher) of analyte are typically used to overcome the reduced sensitivity of TOF instruments in the high mass range. Furthermore, an elevated laser fluence, as well as deviation from optimal preparation protocols, are aggravating effects. It is, therefore, very important to clearly differentiate specific from nonspecific interactions, and this is typically achieved by using a known nonbinding/noninteracting control compound. Because of these limitations, the analyses of noncovalent interactions by MALDI are typically qualitative rather than quantitative.

Within these boundary conditions, a number of reports have described the successful detection of several types of noncovalent complexes [113–118]. During the early days of MALDI, high-intensity signals of noncovalent protein complexes

using a nicotinic acid matrix and a laser wavelength of 266 nm were reported, for example of the tetrameric glucose isomerase [119] and a trimeric porin [120]. Comprehensive reviews have been provided by Hillenkamp [121] and Farmer and Caprioli [122] on this subject. In addition, a report by Zehl and Allmaier on the influence of instrumental parameters for the detection of quaternary protein structures starts from a careful review of the state of the art [123], and provides a critical discussion on the above-described problems. These authors used 2,6-dihydroxyacetophenone as (non-acidic) matrix with the addition of ammonium acetate or diammonium citrate (DAC) to adjust the solution conditions to stabilize the protein complexes. By employing these milder preparation conditions, it was possible to directly measure intact hemoglobin complexes from diluted crude blood samples [124]. Another only slightly acidic matrix which tolerates even highly concentrated additive amounts such as DAC is ATT; this was also used to investigate nucleic acids and their noncovalent complexes and adducts [125].

IR-MALDI enables comparably soft desorption processes and is, therefore, more appropriate for noncovalent complex analysis than UV-MALDI. This is reflected by the successful detection of intact double-stranded DNA as well as enzyme–oligosaccharide complexes in combination with glycerol as matrix which were not detectable or underwent significant fragmentation when UV-MALDI was employed [126, 127].

In more recent approaches, ionic liquid matrices have been used for the facilitated detection of intact noncovalent complexes, most probably due to the omitted requirement of intact complex incorporation into the matrix crystals [86].

Some aggravating circumstances such as the first-shot phenomenon can be circumvented by the accumulation of only first shots fired at fresh sample surfaces. As a consequence of these hindered conditions, numerous approaches regarding the investigation of noncovalent complexes use stabilizing chemical crosslinking between the complex partners in combination with high-mass MALDI [122, 128, 129].

It appears, however, that the potential of MALDI in this area is far from being fully explored. Recently, a new approach was presented to investigate the formation and identification of noncovalent complexes, based on the detection of the "intensity fading" of one complex partner upon the addition of increasing amounts of the other [130], rather than a more ambitious verification of the intact complex. This approach avoids problems related to the detection of the intact complex in the high mass range, and can be carried out at analytically relevant micromolar and submicromolar concentration levels. Up-to-date overviews debating the challenges of mass spectrometric detection of noncovalent interactions, including new developments and chemical crosslinking, have been presented by Bich and Zenobi [131] and Mädler *et al.* [132].

In summary, the use of MALDI to investigate noncovalent interaction is far less straightforward than typical applications for peptides and proteins under denaturing conditions. Success is not predictable, and careful control experiments must be implemented to differentiate specific from nonspecific interactions.

1.8 The Optimal Choice of Matrix: Sample Preparation

Unfortunately – but expectedly – there is no single MALDI matrix or sample preparation protocol which is suited to all analytical problems and analytes in MALDI-MS. A few of the more general considerations are discussed in the following section; more specific information is provided in the applications chapters of this book. A representative list of commonly used matrices and their main applications is provided in Table 1.1.

There are different matrices of first choice for different classes of analytes and analytical problems. For example, HCCA is used in the majority of proteomics applications for the analysis of peptide-mass-fingerprints generated by protein enzymatic digests, as well as for MS/MS fragmentation experiments (as discussed in Chapter 3). The recently discovered ClCCA even improves this performance especially in combination with 337 nm instruments [26, 62]. On the other hand, 2,5-DHB – and especially DHBs (i.e., DHB with an admixture of 5–10% 2-hydroxy-5-methoxybenzoic acid) – with its pronounced crystallization into large crystals of approximately 100 µm size is particularly suited to protein analysis. The reasons for this are: (i) that its softness prevents strong small-neutral losses and peak tailing; and (ii) that the crystals incorporate the proteins but exclude the majority of common contaminants. In addition, there is a large variety of matrix compounds specifically useful for the sensitive detection of specific analyte classes, for example, 2-[(2*E*)-3-(4-*tert*-butylphenyl)-2-methylprop-2-enylidene]malononitrile (DCTB) for polymers and fullerenes [133], 9-aminoacridine [134] and para-nitroaniline [135] for lipids, 2-(4′-hydroxybenzeneazo)benzoic acid (HABA)/1,1,3,3-tetramethylguanidine (TMG) ionic liquid matrices (ILMs) for the intact analysis of heparin sulfate oligosaccharides [136], α-cyano-2,4-difluorocinnamic acid (DiFCCA) [63] and lumazine [137] for phospholipids, an ionic HCCA copper complex for copper-binding peptides [67], or proton sponge for interference-free negative-ion mode analysis of low-mass metabolites [138].

A practical overview of the various matrices and preparation techniques can be found, for example, on the Internet at http://msr.dom.wustl.edu/Research/MALDI_TOF_Mass_Spec_and_Proteomics/MALDI_Sample_Preparation_Methods.htm, as well as on the Internet pages of commercial suppliers of MALDI matrices, for example, http://www.sigmaaldrich.com/analytical-chromatography/analytix-newsletter/analytix-2001.html#analytix6.

The "dried droplet" standard MALDI sample preparation is very simple. Here, the sample and matrix are dissolved in solvents or solvent systems that are miscible with each other, and mixed either before deposition onto or directly on the MALDI sample support. The matrix–analyte droplet of typically 1 µl volume is then slowly dried in air, or under a forced flow of cold air. This results in a deposit of crystals which, depending on the matrix and preparation conditions (e.g., solvent evaporation rate), vary between submicrometer and several hundred micrometers in size. In cases of solvent systems with a high polarity, surface tension leads to a nonhomogeneous distribution of the individual crystals near the rim of the

Table 1.1 A selection of commonly used MALDI matrices.

Matrix	Structure	Wavelength	Major applications
6-Aza-2-thiothymine (ATT)	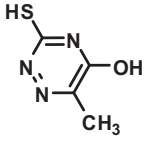	UV 337 nm, 355 nm	Proteins, peptides, noncovalent complexes; near-neutral pH
4-Chloro-α-cyanocinnamic acid (ClCCA)	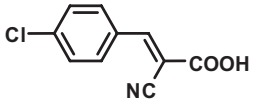	UV 337 nm, (355 nm)	(Glyco/Phospho) Peptides, (halogenated) lipids, fragmentation
α-Cyano-4-hydroxy-cinnamic acid (HCCA)	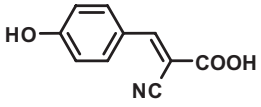	UV 337 nm, 355 nm	Peptides, fragmentation
2,5-Dihydroxybenzoic acid (plus 10% 2-hydroxy-5-methoxy-benzoic acid) (2,5-DHB(s))	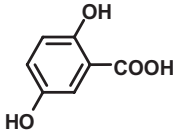	UV 337 nm, 355 nm	Proteins, peptides, carbohydrates, synthetic polymers
k,m,n-Di/Trihydroxy-acetophenone (D/THAP)	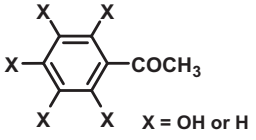	UV 337 nm, 355 nm	Proteins, peptides, noncovalent complexes; near-neutral pH
Glycerol	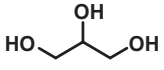	IR 2.94 µm, 2.79 µm	Proteins, peptides; liquid matrix
3-Hydroxypicolinic acid (3-HPA)	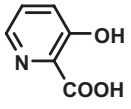	UV 337 nm, 355 nm	Nucleic acids
Nicotinic acid (NA)	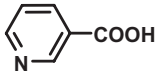	UV 266 nm	Proteins, peptides, adduct formation
Sinapic acid (SA)	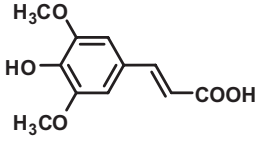	UV 337 nm, 355 nm	Proteins, peptides
Succinic acid	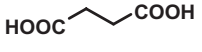	IR 2.94 µm, 2.79 µm	Proteins, peptides

IR, infrared; UV, ultraviolet.

preparation; this led to the development of crystal positioning/detection systems for automated MS measurements in modern MALDI mass spectrometers. The best MALDI performance for classic crystalline matrix preparations is usually achieved only at certain locations of the crystals, which often requires manual interference and active control by the experimenter; this is why most MALDI instruments are equipped with a microscopic sample observation system. The cause of these "sweet spots" has been the subject of much speculation, the commonly held notion being that of an inhomogeneous distribution of analyte within the crystals. However, this has been disproved by Horneffer *et al.*, who found a homogeneous distribution of fluorescently labeled analytes in the crystals of a representative number of different matrix crystals by CLSM studies (see Section 1.2), as well as by Qiao *et al.*, who detected uniformly incorporated proteins in DHB and sinapic acid by means of highly spatially resolved MALDI imaging and fluorescence microscopy [139]. A different (ionization) state of the analyte molecules in different locations, local differences in matrix–analyte interactions [140], as well as different matrix crystallizations due to variations of the local analyte concentrations [141] or heterogeneous orientation of the matrix crystal surfaces relative to the spectrometer axis and perpendicular to which the ions are ejected in conjunction with the limited angular acceptance of the mass spectrometer, might also cause the observed sweet spots.

As a rule of thumb, addition of the analyte solution should not noticeably change the crystallization behavior of the neat matrix; an unchanged morphology already indicates that the solution excess of the matrix with respect to the analyte is maintained in the crystals, and that the contaminant level is low. Any solute component which already at low concentrations dramatically changes the morphology of the subsequently crystallized matrix or prevents crystallization altogether – for example, low-volatility solvents such as dimethyl sulfoxide or common detergents – will prohibit a successful MALDI analysis.

Over the years, a large number of modifications of, or alternatives to, the dried-droplet technique have been developed. These many variations are often the personal preferences of MALDI users for sample preparation, and the subject may appear to be an art, or even a "black art." Nonetheless, dried-droplet sample preparations are still most widely used with high success due to their simple and rapid handling. It also appears that instrumental developments using lasers with higher frequencies (e.g., modern Nd:YAG solid-state lasers with repetition rates of up to 1 kHz), together with the automation of entire MALDI measurements, have eased the problems of heterogeneity to some extent. Additionally, modifications of the dried-droplet preparation such as, for example, a rapid evaporation of the solvent of standard dried-droplet preparations by reduced pressure [142] or the rapid-evaporation crystallization by using highly volatile solvents such as acetone [143], both result in smaller and more homogeneously distributed crystals with improved spot-to-spot reproducibilities and minimized sweet spots.

Among the many modifications and variations of the simple dried-droplet preparation, two alternatives stand out as particularly useful and widespread, namely "surface preparation" and "anchor sample plates."

1.8.1 Surface Preparation

Surface preparations or predeposited matrix crystal layers are also often called thin-layer or two-layer preparations, and were introduced to enhance sensitivity, homogeneity of the preparation, automation, and liquid chromatography (LC)-spotting.

Surface preparation was a true innovation [144]. As discussed above for the rapid-evaporation crystallization, the HCCA matrix generates a relatively homogeneous microcrystalline layer upon rapid evaporation of the organic solvent. Subsequent addition of the aqueous peptide analyte solution – which must contain a low amount of organic solvent – redissolves only the very top layers of the near-water-insoluble matrix and incorporates and concentrates the analyte upon recrystallization using the nondissolved matrix bed as seed crystals [145]. It has been shown that the addition of a low matrix amount to the analyte solution (containing a somewhat higher organic solvent amount) to be applied onto the microcrystalline matrix layer increases the achievable sensitivity for proteins. The structurally relatively homogeneous sample surface further increases the mass resolution, particularly in linear TOF mass spectrometers.

Unfortunately, this approach is restricted to matrices which do not fully dissolve in the usually aqueous analyte solvent. However, despite its limited solubility, the matrix is partially dissolved by the analyte solution, and true incorporation of the analyte into the matrix takes place. It was shown, moreover, that contaminants such as salts could be rinsed from the surface with a splash of ice water, without causing any major analyte loss which results in clearly higher sensitivities. Hence, surface preparation became the starting point for the development of disposable MALDI targets with predeposited matrix spots [146]. The generation of more homogeneous microcrystalline sample layers by rapid evaporation of the solvent (e.g., *in vacuo*) has also been used for a variety of other matrices (Figure 1.5).

1.8.2 Anchor Sample Plates

Anchor plates for the preparation of multiple samples have small hydrophilic islands, typically of 100–500 µm diameter, placed on a hydrophobic surface [147]. The hydrophobic surface prevents spreading of the sample solution over a larger area, as otherwise observed for dried-droplet preparations. Instead, the hydrophilic solution contracts onto these islands, thereby concentrating the matrix and analyte onto a small defined area upon solvent evaporation. This confinement to a smaller volume is particularly useful for analytes of low concentration in combination with proportionally lowered matrix concentrations, and also facilitates automated analyses of the fixed-location samples. Anchor sample plates are also commercially available as disposable targets prespotted with matrix and calibration spots.

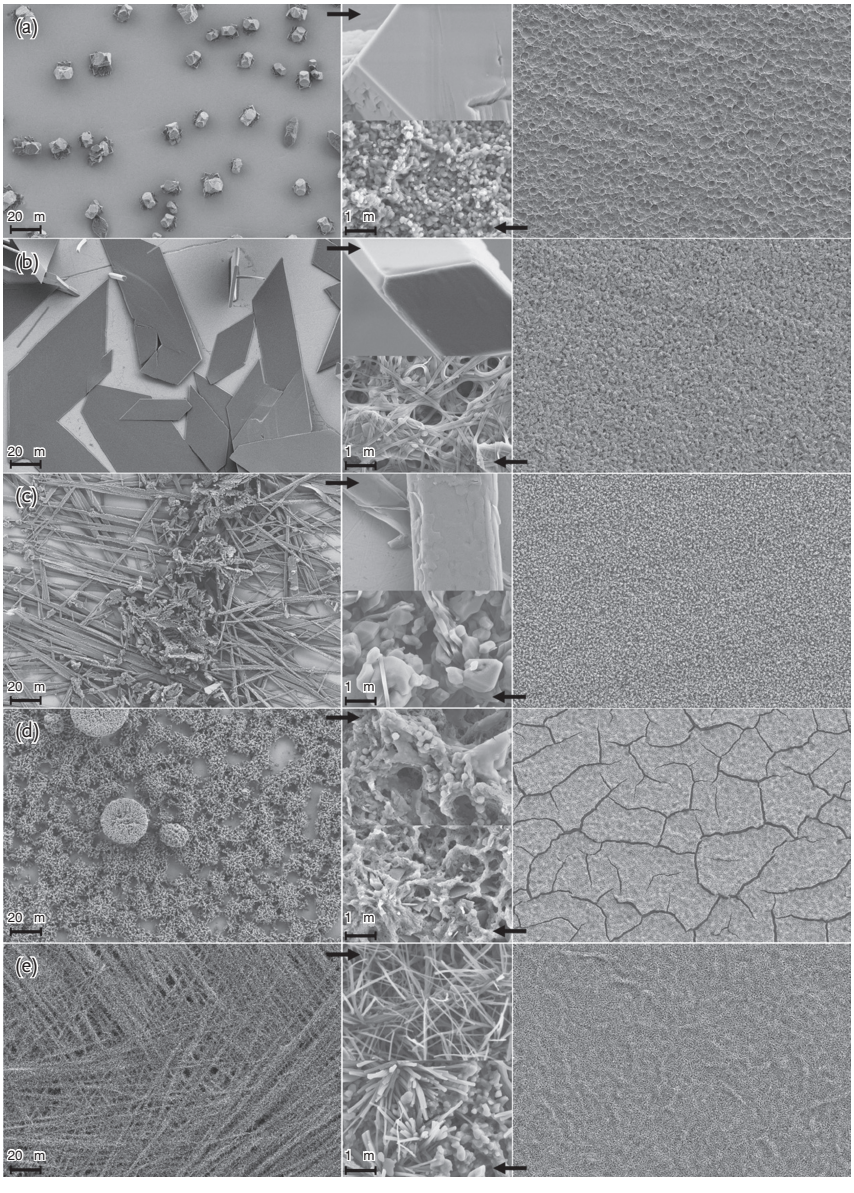

Figure 1.5 Matrix crystals resulting from standard dried-droplet preparations on stainless steel plate (left) and from sublimed preparations on hydrophobically coated aluminum oxide surfaces (right). From upper to lower: (a) HCCA; (b) sinapic acid, (c) 4-methyl-CCA; (d) 4-hydroxy-3-methyl-CCA; (e) 4-hydroxy-3-methoxy-CCA. Image reproduced from Ref. [145] with permission from Elsevier.

1.8.3 Matrix Additives and Influence of the Sample Plate Surface

A few other modifications of the sample preparation have also proven useful in specific cases:

- Mixtures of several different matrices have been reported for an improved performance, for example, 1:1 (w/w) mixtures between HCCA and DHB resulted in a lowered chemical noise and slightly improved sequence coverages [148]. However, so far only DHBs (a mixture of 90–95% 2,5-DHB and 5–10% 2-hydroxy-5-methoxybenzoic acid) has found relatively widespread application for proteins [149]. The additive softens the desorption and limits the small neutral loss, thereby improving mass resolution. A mixture of different trihydroxyacetophenones is sometimes used for the analysis of nucleic acids [150].
- Additives to matrix preparations are mostly used for intrinsic sample clean-up. These additives do not absorb the laser radiation but may influence the crystallization behavior of the matrix to some extent as a side effect. The most frequently used method is to add diammonium citrate (DAC) as a cation scavenger to preparations of highly anionic samples such as nucleic acids containing high amounts of alkali metal counterions [151]. The addition of ammonium phosphate to improve peptide-fingerprint mass spectra by the suppression of matrix cation clusters, and the use of up to 1% phosphoric acid to improve DHB analysis of phosphopeptides, may be due to a more efficient incorporation of positively precharged phosphopeptides with neutral phosphate groups into the growing matrix crystals, are two recent successful examples of this approach [152, 153].

Modified surfaces of sample plates can be used for the affinity capture of analytes from crude mixtures directly on target. Such surfaces can significantly enhance detection sensitivity and can be used for simple sample clean-ups. Titania (TiO_2)-coated surfaces, particles or sol–gel systems, for example, have been shown to concentrate phosphopeptides very selectively from peptide fingerprint samples [154, 155].

Surface-enhanced laser desorption ionization (SELDI) uses so-called "protein chips" for the detection of peptides and proteins from complex biological fluids such as blood or urine, often for the identification of diagnostic biomarkers for specific carcinomas [156, 157]. These protein chips can contain various media for positive or negative ion exchange or reverse-phase chromatography, as well as specific antibodies or DNA. The functionalized surface is immobilized on a MALDI sample plate for the selective enrichment of constituents of the complex mixture applied, whereas the not bound supernatant is removed by washing. Unfortunately, a large number of unsubstantiated claims for the detection of disease-related biomarkers has discredited this approach, mostly as a result of poor mass spectrometric performance.

Liquid matrices can avoid the undesirable heterogeneity of crystalline MALDI samples. Liquid matrices (e.g., nitrobenzylalcohol and nitrophenyloctylether)

were introduced in the early UV-MALDI reports, but never found widespread application because their performance proved to be significantly inferior to that of the traditional solid matrices, particularly because of extensive adduct formation. A more recent development has been the synthesis of ILMs, which are synthesized by preparing a 1 : 1 solution of a classical organic acid matrix with an organic base, for example, pyridine or 3-aminoquinoline [158]. Such preparations allow for higher shot-to-shot- as well as spot-to-spot-reproducibility compared to crystalline matrices, although their sensitivities are typically lowered. Unfortunately, the most sensitive ILMs are either solid or very highly viscous liquids. A possible solution to this problem is the addition of a polar liquid of low volatility, such as glycerol, which would stabilize the generated ion-pairs and alleviate liquid preparations [159]. Such liquid-support matrices exhibit high analyte homogeneities with nearly constant ion signal intensities across the whole preparation [160].

To date, these types of matrices seem to be mostly restricted to the MALDI-MS analysis and the quantification of small, stable analytes. Nevertheless, recent optimization approaches using sterically hindered bases such as *N*,*N*-diisopropylethylamine or *N*-isopropyl-*N*-methyl-*N*-*tert*-butylamine also allow for the detection of high-molecular-weight analytes such as large proteins [86]. Today, ILMs are becoming increasingly important for imaging MALDI-MS, due to their homogeneous sample surface coverage going along with the elimination of the hot-spot phenomenon [161, 162]. Further information regarding sample preparation and the effects of specific bases, as well as additional application areas, is provided in Refs [140, 163].

A solvent-free preparation is of particular interest for the analysis of synthetic polymers for which a common solvent with a suitable matrix is not available, and for which sizeable amounts of material are usually on hand [164]. In this protocol, the mixed analyte, matrix, and often a cationizing compound (e.g., AgCl or NaCl) are ground thoroughly in a mortar or ball-mill and loaded onto a MALDI target as powders, or after having been pressed into pellets. Good mass spectra can be obtained for analytes up to a mass of ca. 30 kDa, even though the analytes are not incorporated into the matrix crystals [35].

Abbreviations

5-ASA	5-Aminosalicylic acid
ATT	6-Aza-2-thiothymine
CCA	α-Cyanocinnamic acid
CID	Collisional induced dissociation
ClCCA	4-Chloro-α-cyanocinnamic acid
CLSM	Confocal laser scan microscopy
DAC	Diammonium citrate
1,5-DAN	1,5-Diaminonaphthalene
DCTB	2-[(2*E*)-3-(4-*tert*-butylphenyl)-2-methylprop-2-enylidene] malononitrile
DHB/2,5-DHB	(2,5-)Dihydroxybenzoic acid
2,6-DHB	2,6-Dihydroxybenzoic acid

DHBs	"super" DHB (mixture of 90–95% DHB and 5–10% 2-hydroxy-5-methoxybenzoic acid)
DiFCCA	α-Cyano-2,4-difluorocinnamic acid
DIOS	Desorption/ionization on silicon
ESI	Electrospray ionization
FA	Formic acid
FAB	Fast atom bombardment
FD	Field desorption
FRET	Fluorescence resonant energy transfer
HABA	2-(4-Hydroxyphenylazo)benzoic acid
HCCA	α-Cyano-4-hydroxycinnamic acid
3-HPA	3-Hydroxypicolinic acid
ILM	Ionic liquid matrix
IR	Infrared
ISD	In-source decay
LAMMA	Laser microprobe mass analyzer
LC	Liquid chromatography
MALDI	Matrix-assisted laser desorption/ionization
AP-MALDI	MALDI at atmospheric pressure
IR-MALDI	MALDI with infrared laser wavelengths
UV-MALDI	MALDI with ultraviolet laser wavelengths
MS	Mass spectrometry
MSA	2-Hydroxy-5-methoxysalicylic acid
OPO	Optical parametric oscillator
PA	Proton affinity
PD	Plasma desorption
PSD	Post-source decay
SALDI	Surface-assisted laser desorption/ionization
SELDI	Surface-enhanced laser desorption/ionization
SIMS	Secondary ion mass spectrometry
TFA	Trifluoroacetic acid
TMG	1,1,3,3-Tetramethylguanidine
TOF	Time-of-flight
TOF-MS	Time-of-flight mass spectrometer
UV	Ultraviolet

References

1 Deisewerd, K. (2003) The desorption process in MALDI. *Chem. Rev.*, **103**, 395–425.

2 Karas, M. and Krüger, R. (2003) Ion formation in MALDI. *Chem. Rev.*, **103**, 427–439.

3 Knochenmuss, R. and Zenobi, R. (2003) MALDI ionization: the role of in-plume processes. *Chem. Rev.*, **103**, 441–452.

4 El-Aneed, A., Cohen, A., and Banoub, J. (2009) Mass spectrometry, review of the basics: electrospray, MALDI, and commonly used mass analyzers. *Appl. Spectrosc. Rev.*, **44**, 210–230.

5 Beckey, H.D. (1977) *Principles of Field Ionization and Field Desorption Mass Spectrometry, International Series in Analytical Chemistry*, Pergamon Press.

6 Benninghoven, A. and Sichtermann, W. (1978) Detection, identification and structural investigation of biologically important compounds by secondary ion mass spectrometry. *Anal. Chem.*, **50**, 1180–1184.

7 Zakett, D., Schoen, A.E., Cooks, R.G., and Hemberger, P.H. (1981) Laser-desorption mass spectrometry/mass spectrometry and the mechanism of desorption ionization. *J. Am. Chem. Soc.*, **103**, 1295–1297.

8 Torgerson, D.F., Skrowonski, R.P., and Macfarlane, R.D. (1974) New approach to the mass spectroscopy of nonvolatile compounds. *Biochem. Biophys. Res. Commun.*, **60**, 616–619.

9 Jonsson, G.P., Hedin, A.B., Håkansson, P.L., Sundqvist, B.U.R., Save, B.G., Nielsen, P.F., Roepstorff, P., Johansson, K.E., Kamensky, I., and Lindberg, M.S. (1986) Plasma desorption mass spectrometry of peptides and proteins adsorbed on nitrocellulose. *Anal. Chem.*, **58**, 1084–1087.

10 Fenner, N.C. and Daly, N.R. (1966) Laser used for mass analysis. *Rev. Sci. Instrum.*, **37**, 1068–1072.

11 Vastola, F.J., Mumma, R.O., and Pirone, A.J. (1970) Analysis of organic salts by laser ionization. *Org. Mass Spectrom.*, **3**, 101–104.

12 Posthumus, N.A., Kistemaker, P.G., Meuzelaar, H.L.C., and Ten Noever de Brauw, M.C. (1978) Laser desorption-mass spectrometry of polar nonvolatile bioorganic molecules. *Anal. Chem.*, **50**, 985–991.

13 Hillenkamp, F., Kaufmann, R., Nitsche, R., and Unsöld, E. (1975) Laser microprobe mass analysis of organic materials. *Nature*, **256**, 119–120.

14 Karas, M., Bachmann, D., and Hillenkamp, F. (1985) Influence of the wavelength in high-irradiance ultraviolet laser desorption mass spectrometry of organic molecules. *Anal. Chem.*, **57**, 2935–2939.

15 Hillenkamp, F. (1986) Laser desorption mass spectrometry. A review, in *Secondary Ion Mass Spectrometry SIMS V. Springer Series in Chemical Physics*, vol. 44 (eds A. Benninghoven, R.J. Colton, D.S. Simons, and H.W. Werner), Springer-Verlag, Berlin, pp. 471–475.

16 Karas, M. and Hillenkamp, F. (1988) Laser desorption ionization of proteins with molecular masses exceeding 10 000 daltons. *Anal. Chem.*, **60**, 2299–2301.

17 Tanaka, K., Waki, H., Ido, Y., Akita, S., Yoshida, Y., and Yoshida, T. (1988) Protein and polymer analyses up to m/z 100 000 by laser ionization time-of-flight mass spectrometry. *Rapid Commun. Mass Spectrom.*, **2**, 151–153.

18 Schürenberg, M., Dreisewerd, K., and Hillenkamp, F. (1999) Laser desorption/ionization mass spectrometry of peptides and proteins with particle suspension matrixes. *Anal. Chem.*, **71**, 221–229.

19 Sunner, J., Dratz, E., and Chen, Y.-C. (1995) Graphite surface-assisted laser desorption/ionization time-of-flight mass spectrometry of peptides and proteins from liquid solutions. *Anal. Chem.*, **67**, 4335–4342.

20 Wei, J., Buriak, J.M., and Siuzdak, G. (1999) Desorption–ionization mass spectrometry on porous silicon. *Nature*, **399**, 243–246.

21 Trauger, S.A., Go, E.P., Shen, Z., Apon, J.V., Compton, B.J., Bouvier, E.S.P., Finn, M.G., and Siuzdak, G. (2004) High sensitivity and analyte capture with desorption/ ionization mass spectrometry on silylated porous silicon. *Anal. Chem.*, **76**, 4484–4489.

22 Trimpin, S., Inutan, E.D., Herath, T.N., and McEwen, C.N. (2010) Laserspray ionization, a new atmospheric pressure MALDI method for producing highly charged gas-phase ions of peptides and proteins directly from solid solutions. *Mol. Cell. Proteomics*, **9**, 362–367.

23 Trimpin, S., Wang, B., Inutan, E.D., Li, J., Lietz, C.B., Harron, A., Pagnotti, V.S., Sardelis, D., and McEwen, C.N. (2012) A mechanism for ionization of nonvolatile compounds in mass spectrometry: considerations from MALDI and inlet ionization. *J. Am. Soc. Mass Spectrom.*, **23**, 1644–1660.

24 Jaskolla, T.W. and Karas, M. (2011) Compelling evidence for lucky survivor and gas phase protonation: the unified MALDI analyte protonation mechanism. *J. Am. Soc. Mass Spectrom.*, **22**, 976–988.

25 Soltwisch, J., Jaskolla, T.W., Hillenkamp, F., Karas, M., and Dreisewerd, K. (2012)

Ion yields in UV-MALDI mass spectrometry as a function of excitation laser wavelength and optical and physico-chemical properties of classical and novel halogen-substituted MALDI matrices. *Anal. Chem.*, **84**, 6567–6576.

26 Jaskolla, T.W., Lehmann, W.-D., and Karas, M. (2008) 4-Chloro-α-cyanocinnamic acid is an advanced, rationally designed MALDI matrix. *Proc. Natl. Acad. Sci. USA*, **105**, 12200–12205.

27 Strupat, K., Karas, M., and Hillenkamp, F. (1991) 2,5-Dihydroxybenzoic acid: a new matrix for laser desorption-ionization mass spectrometry. *Int. J. Mass Spectrom. Ion Processes*, **111**, 89–102.

28 Beavis, R.C. and Bridson, J.N. (1993) Epitaxial protein inclusion in sinapic acid crystals. *Appl. Phys.*, **26**, 442–447.

29 Horneffer, V. (2002) Matrix-Analyt-Wechselwirkungen bei der Matrix-Unterstützten Laserdesorptions/ionisations Massenspektrometrie (MALDI-MS). Dissertation, University of Münster.

30 Kampmeier, J., Dreisewerd, K., Schürenberg, M., and Hillenkamp, F. (1997) Investigations of 2,5-DHB and succinic acid as matrices for IR and UV MALDI: part 1: UV and IR laser ablation in the MALDI process. *Int. J. Mass Spectrom. Ion Processes*, **169/170**, 31–41.

31 Krueger, R., Pfenninger, A., Fournier, I., Glückmann, M., and Karas, M. (2001) Analyte incorporation and ionization in matrix-assisted laser desorption/ionization visualized by pH indicator molecular probes. *Anal. Chem.*, **73**, 5812–5821.

32 Horneffer, V., Forsmann, A., Strupat, K., Hillenkamp, F., and Kubitschek, U. (2001) Localization of analyte molecules in MALDI preparations by confocal laser scanning microscopy. *Anal. Chem.*, **73**, 1016–1022.

33 Horneffer, V., Reichelt, R., and Strupat, K. (2003) Protein incorporation into MALDI-matrix crystals investigated by high resolution field emission scanning electron microscopy. *Int. J. Mass Spectrom.*, **226**, 117–131.

34 Skelton, R., Dubois, F., and Zenobi, R. (2000) A MALDI sample preparation method suitable for insoluble polymers. *Anal. Chem.*, **72**, 1707.

35 Horneffer, V., Glückmann, M., Krüger, R., Karas, M., Strupat, K., and Hillenkamp, F. (2006) Matrix-analyte-interaction in MALDI-MS: pellet and nano-electrospray preparations. *Int. J. Mass Spectrom.*, **249/250**, 426–432.

36 Dreisewerd, K., Schürenberg, M., Karas, M., and Hillenkamp, F. (1995) Influence of the laser intensity and spot size on the desorption of molecules and ions in matrix-assisted laser desorption/ionization with a uniform beam profile. *Int. J. Mass Spectrom. Ion Processes*, **141**, 127–148.

37 Lüdemann, H.-C., Redmond, R.W., and Hillenkamp, F. (2002) Singlet-singlet annihilation in UV-MALDI studied by fluorescence spectroscopy. *Rapid Commun. Mass Spectrom.*, **16**, 1287–1294.

38 Knochenmuss, R. (2004) Photoionization pathways and free electrons in UV-MALDI. *Anal. Chem.*, **76**, 3179–3184.

39 Dreisewerd, K. (2003) The desorption process in MALDI. *Chem. Rev.*, **103**, 395–425.

40 Zhigilei, L.V. and Garrison, B. (2000) Microscopic mechanisms of laser ablation of organic solids in the thermal and stress confinement irradiation regimes. *J. Appl. Phys.*, **88**, 1281–1298.

41 Rohlfing, A., Menzel, C., Kukreja, L.M., Hillenkamp, F., and Dreisewerd, K. (2003) Photoacoustic analysis of matrix-assisted laser desorption/ionization processes with pulsed infrared lasers. *J. Phys. Chem. B*, **107**, 12275–12286.

42 Leisner, A., Rohlfing, A., Röhling, U., Dreisewerd, K., and Hillenkamp, F. (2005) Time-resolved imaging of the plume dynamics in infrared matrix-assisted laser desorption/ionization with a glycerol matrix. *J. Phys. Chem. B*, **109**, 11661–11666.

43 Menzel, C., Dreisewerd, K., Berkenkamp, S., and Hillenkamp, F. (2002) The role of the laser pulse duration in infrared matrix-assisted laser desorption/ionization mass spectrometry. *J. Am. Soc. Mass Spectrom.*, **13**, 975–984.

44 Rohlfing, A. (2006) Untersuchungen zum Desorptionsprozess in der UV-Matrix-unterstützten Laserdesorption/-ionisation mit einer Flüssigmatrix. Dissertation, University of Münster.

45 Vogel, A. and Venugopalan, V. (2003) Mechanisms of pulsed laser ablation of biological tissues. *Chem. Rev.*, **103**, 577–644.

46 Kelly, R. and Miotello, A. (1999) Contribution of vaporization and boiling to thermal-spike sputtering by ions or laser pulses. *Phys. Rev. E*, **60**, 2616–2625.

47 Alves, S., Kalberer, M., and Zenobi, R. (2003) Direct detection of particles formed by laser ablation of matrices during matrix-assisted laser desorption/ionization. *Rapid Commun. Mass Spectrom.*, **17**, 2034–2038.

48 Hoyer, T., Tuszynski, W., and Lienau, C. (2007) Ultrafast photodimerization dynamics in a-cyano-4-hydroxycinnamic acid and sinapinic acid crystals. *Chem. Phys. Lett.*, **443**, 107–112.

49 Sachon, E., Clodic, G., Blasco, T., and Bolbach, G. (2007) Protein desolvation in UV matrix-assisted laser desorption/ionization (MALDI). *J. Am. Soc. Mass Spectrom.*, **18**, 1880–1890.

50 Zhigilei, L.V. and Garrison, B.J. (1999) Mechanisms of laser ablation from molecular dynamics simulation: dependence on the initial temperature and pulse duration. *Appl. Phys. A*, **69**, 75–80.

51 Zhigilei, L.V., Kodali, P.B.S., and Garrison, B.J. (1998) A microscopic view of laser ablation. *J. Phys. Chem. B*, **102**, 2845–2853.

52 Lin, Q. and Knochenmuss, R. (2001) Two-photon ionization thresholds of matrix-assisted laser desorption/ionization matrix clusters. *Rapid Commun. Mass Spectrom.*, **15**, 1422–1426.

53 Setz, P.D. and Knochenmuss, R. (2005) Exciton mobility and trapping in a MALDI matrix. *J. Phys. Chem. A*, **109**, 4030–4037.

54 Ehring, H., Karas, M., and Hillenkamp, F. (1992) Role of photoionization and photochemistry in ionization processes of organic molecules and relevance for matrix-assisted laser desorption ionization mass spectrometry. *Org. Mass Spectrom.*, **27**, 472–480.

55 Mowry, C.D. and Johnston, M.V. (1993) Simultaneous detection of ions and neutrals produced by matrix-assisted laser desorption. *Rapid Commun. Mass Spectrom.*, **7**, 569–575.

56 Quist, A.P., Huth-Fehre, T., and Sundqvist, B.U.R. (1994) Total yield measurements in matrix-assisted laser desorption using a quartz crystal microbalance. *Rapid Commun. Mass Spectrom.*, **8**, 149–154.

57 Knochenmuss, R., Dubois, F., Dale, M.J., and Zenobi, R. (1996) The matrix suppression effect and ionization mechanisms in matrix-assisted laser desorption/ionization. *Rapid Commun. Mass Spectrom.*, **10**, 871–877.

58 Knochenmuss, R. and Zhigilei, L.V. (2010) Molecular dynamics simulations of MALDI: laser fluence and pulse width dependence of plume characteristics and consequences for matrix and analyte ionization. *J. Mass Spectrom.*, **45**, 333–346.

59 Friess, S.D. and Zenobi, R. (2001) Protein structure information from mass spectrometry? selective titration of arginine residues by sulfonates. *J. Am. Soc. Mass Spectrom.*, **12**, 810–818.

60 Krüger, R. and Karas, M. (2002) Formation and fate of ion pairs during MALDI analysis: anion adduct generation as an indicative tool to determine ionization processes. *J. Am. Soc. Mass Spectrom.*, **13**, 1218–1226.

61 Jørgensen, T.J.D., Bojesen, G., and Rahbek-Nielsen, H. (1998) The proton affinities of seven matrix-assisted laser desorption/ionization matrices correlated with the formation of multiply charged ions. *Eur. J. Mass Spectrom.*, **4**, 39–45.

62 Jaskolla, T.W., Papasotiriou, D.G., and Karas, M. (2009) Comparison between the matrices α-cyano-4-hydroxycinnamic acid and 4-chloro-α-cyanocinnamic acid for trypsin, chymotrypsin, and pepsin digestions by MALDI-TOF mass spectrometry. *J. Proteome Res.*, **8**, 3588–3597.

63 Teuber, K., Schiller, J., Fuchs, B., Karas, M., and Jaskolla, T.W. (2010) Significant

sensitivity improvements by matrix optimization: a MALDI-TOF mass spectrometric study of lipids from hen egg yolk. *Chem. Phys. Lipids*, **163**, 552–560.

64 Harrison, A.G. (1997) The gas-phase basicities and proton affinities of amino acids and peptides. *Mass Spectrom. Rev.*, **17**, 201–217.

65 Knochenmuss, R. (2006) Ion formation mechanisms in UV-MALDI. *Analyst*, **131**, 966–986.

66 Pfenninger, A., Karas, M., Finke, B., Stahl, B., and Sawatzki, G. (1999) Matrix optimization for matrix-assisted laser desorption/ionization mass spectrometry of oligosaccharides from human milk. *J. Mass Spectrom.*, **34**, 98–104.

67 Wu, Z., Fernandez-Lima, F.A., Perez, L.M., and Russell, D.H. (2009) A new copper containing MALDI matrix that yields high abundances of $[peptide + Cu]^+$ ions. *J. Am. Soc. Mass Spectrom.*, **20**, 1263–1271.

68 Karas, M., Bahr, U., Hillenkamp, F., Tsarbopoulos, A., and Pramanik, B.N. (1995) Matrix dependence of metastable fragmentation of glycoproteins in MALDI TOF mass spectrometry. *Anal. Chem.*, **67**, 675–679.

69 Spengler, B., Kirsch, D., and Kaufmann, R. (1992) Fundamental aspects of post-source decay in MALDI mass spectrometry. *J. Phys. Chem.*, **96**, 9678–9684.

70 Spengler, B. (1997) Post-source decay analysis in matrix-assisted laser desorption/ionization mass spectrometry of biomolecules. *J. Mass Spectrom.*, **32**, 1019–1036.

71 Chaurand, P., Luetzenkirchen, F., and Spengler, B. (1999) Peptide and protein identification by matrix-assisted laser desorption ionization (MALDI) and MALDI-post-source decay time-of-flight mass spectrometry. *J. Am. Soc. Mass Spectrom.*, **10**, 91–103.

72 Suckau, D., Resemann, A., Schuerenberg, M., Hufnagel, P., Franzen, J., and Holle, A. (2003) A novel MALDI LIFT-TOF/TOF mass spectrometer for proteomics. *Anal. Bioanal. Chem.*, **376**, 952–965.

73 Vestal, M. and Hayden, K. (2012) A new approach to TOF mass spectrometry for high performance MS and MS-MS. Proceedings, 60th Annual ASMS Conference on Mass Spectrometry and Allied Topics, Vancouver, BC, Canada, May 20–24, 2012.

74 Harvey, D.J. (1999) Matrix-assisted laser desorption/ionization mass spectrometry of carbohydrates. *Mass Spectrom. Rev.*, **18**, 349–451.

75 Zhang, L. and Reilly, J.P. (2009) Extracting both peptide sequence and glycan structural information by 157 nm photodissociation of N-linked glycopeptides. *J. Proteome Res.*, **8**, 734–742.

76 Stevenson, E., Breuker, K., and Zenobi, R. (2000) Internal energies of analyte ions generated from different matrix-assisted laser desorption/ionization matrices. *J. Mass Spectrom.*, **35**, 1035–1041.

77 Demeure, K., Gabelica, V., and De Pauw, E.A. (2010) New advances in the understanding of the in-source decay fragmentation of peptides in MALDI-TOF-MS. *J. Am. Soc. Mass Spectrom.*, **21**, 1906–1917.

78 Gabelica, V., Schulz, E., and Karas, M. (2004) Internal energy build-up in matrix-assisted laser desorption/ionization. *J. Mass Spectrom.*, **39**, 579–593.

79 Luo, G., Marginean, I., Ye, L., and Vertes, A. (2008) Competing ion decomposition channels in matrix-assisted laser desorption ionization. *J. Phys. Chem. B*, **11**, 6952–6956.

80 Yoon, S.H., Moon, J.H., and Kim, M.S. (2010) A comparative study of in- and post-source decays of peptide and preformed ions in matrix-assisted laser desorption ionization time-of-flight mass spectrometry: effective temperature and matrix effect. *J. Am. Soc. Mass Spectrom.*, **21**, 1876–1883.

81 Schulz, E., Karas, M., Rosu, F., and Gabelica, V. (2006) Influence of the matrix on analyte fragmentation in atmospheric pressure MALDI. *J. Am. Soc. Mass Spectrom.*, **17**, 1005–1013.

82 Bae, Y.J., Moon, J.H., and Kim, M.S. (2011) Expansion cooling in the matrix

plume is under-recognized in MALDI mass spectrometry. *J. Am. Soc. Mass Spectrom.*, **22**, 1070–1078.

83 Leszyk, J.D. (2010) Evaluation of the new MALDI matrix 4-chloro-α-cyanocinnamic acid. *J. Biomol. Tech.*, **21**, 81–91.

84 Glückmann, M. and Karas, M. (1999) The initial ion velocity and its dependence on matrix, analyte and preparation method in ultraviolet matrix-assisted laser desorption/ionization. *J. Mass Spectrom.*, **34**, 467–477.

85 Bahr, U., Stahl-Zeng, J., Gleitsmann, E., and Karas, M. (1997) Delayed extraction time-of-flight MALDI mass spectrometry of proteins above 25 000 Da. *J. Mass Spectrom.*, **32**, 1111–1116.

86 Crank, J.A. and Armstrong, D.W. (2009) Towards a second generation of ionic liquid matrices (ILMs) for MALDI-MS of peptides, proteins, and carbohydrates. *J. Am. Soc. Mass Spectrom.*, **20**, 1790–1800.

87 Kaufmann, R., Kirsch, D., and Spengler, B. (1994) Sequencing of peptides in a time-of-flight mass spectrometer: evaluation of postsource decay following matrix-assisted laser desorption ionization (MALDI). *Int. J. Mass Spectrom. Ion Processes*, **131**, 355–385.

88 Brown, R.S., Carr, B.L., and Lennon, J.L. (1996) Factors that influence the observed fast fragmentation of peptides in matrix-assisted laser desorption. *J. Am. Soc. Mass Spectrom.*, **7**, 225–232.

89 Reiber, D.C., Brown, R.S., Weinberger, S., Kenny, J., and Bailey, J. (1998) Unknown peptide sequencing using matrix-assisted laser desorption/ionization and in-source decay. *Anal. Chem.*, **70**, 1214–1222.

90 Brown, R.S., Feng, J., and Reiber, D.C. (1997) Further studies of in-source fragmentation of peptides in MALDI. *Int. J. Mass Spectrom. Ion Processes*, **169/170**, 1–18.

91 Smargiasso, N., Quinton, L., and De Pauw, E. (2012) 2-Aminobenzamide and 2-aminobenzoic acid as new MALDI matrices inducing radical mediated in-source decay of peptides and proteins. *J. Am. Soc. Mass Spectrom.*, **23**, 469–474.

92 Hagan, N.A., Smith, C.A., Antoine, M.D., Lin, J.S., Feldman, A.B., and Demirev, P.A. (2012) Enhanced in-source fragmentation in MALDI-TOF-MS of oligonucleotides using 1,5-diaminonaphthalene. *J. Am. Soc. Mass Spectrom.*, **23**, 773–777.

93 Wang, B.H., Hopkins, C.E., Belenky, A.B., and Cohen, A.S. (1997) Sequencing of modified oligonucleotides using in-source fragmentation and delayed pulsed ion extraction matrix-assisted laser desorption ionization time-of-flight mass spectrometry. *Int. J. Mass Spectrom.*, **169**, 331–350.

94 Yamagaki, T., Suzuki, H., and Tachibana, K. (2005) In-source and post-source decay in negative-ion matrix-assisted laser desorption/ionization time-of-flight mass spectrometry of neutral oligosaccharides. *Anal. Chem.*, **77**, 1701–1707.

95 Takayama, M.N. (2001) N-C_α bond cleavage of the peptide backbone via hydrogen abstraction. *J. Am. Soc. Mass Spectrom.*, **12**, 1044–1049.

96 Demeure, K., Quinton, L., Gabelica, V., and De Pauw, E. (2007) Rational selection of the optimum MALDI matrix for top-down proteomics by in-source decay. *Anal. Chem.*, **79**, 8678–8685.

97 Sakakura, M. and Takayama, M. (2010) In-source decay and fragmentation characteristics of peptides using 5-aminosalicylic acid as a matrix in matrix-assisted laser desorption/ionization mass spectrometry. *J. Am. Soc. Mass Spectrom.*, **21**, 979–988.

98 Fukuyama, Y., Iwamoto, S., and Tanaka, K. (2006) Rapid sequencing and disulfide mapping of peptides containing disulfide bonds by using 1,5-diaminonaphthalene as a reductive matrix. *J. Mass Spectrom.*, **41**, 191–201.

99 Köcher, T., Engström, A., and Zubarev, R.A. (2005) Fragmentation of peptides in MALDI in-source decay mediated by hydrogen radicals. *Anal. Chem.*, **77**, 172–177.

100 Schnaible, V., Wefing, S., Resemann, A., Suckau, D., Bücker, A., Wolf-Kümmeth, S., and Hoffmann, D. (2002) Screening for disulfide bonds in proteins by MALDI in-source decay and LIFT-TOF/TOF-MS. *Anal. Chem.*, **74**, 4980–4988.

101 Asakawa, D. and Takayama, M. (2012) Fragmentation processes of hydrogen-deficient peptide radicals in matrix-assisted laser desorption/ionization in-source decay mass spectrometry. *J. Phys. Chem. B*, **116**, 4016–4023.

102 Reiber, D.C., Grover, T.A., and Brown, R.S. (1998) Identifying proteins using matrix-assisted laser desorption/ionization in-source fragmentation data combined with database searching. *Anal. Chem.*, **70**, 673–683.

103 Takayama, M. and Tsugita, A. (2000) Sequence information of peptides and proteins with in-source decay in matrix assisted laser desorption/ionization-time of flight-mass spectrometry. *Electrophoresis*, **21**, 1670–1677.

104 Calligaris, D., Villard, C., Terras, L., Braguer, D., Verdier-Pinard, P., and Lafitte, D. (2010) MALDI in-source decay of high mass protein isoforms: applications to α- and β-tubulin variants. *Anal. Chem.*, **82**, 6176–6184.

105 Zimmerman, T.A., Debois, D., Mazzucchelli, G., Bertrand, V., De Pauw-Gillet, M.-C., and De Pauw, E. (2011) An analytical pipeline for MALDI in-source decay mass spectrometry imaging. *Anal. Chem.*, **83**, 6090–6097.

106 Rosinke, B., Strupat, K., Hillenkamp, F., Rosenbusch, J., Dencher, N., Krüger, U., and Galla, H.-J. (1995) Matrix-assisted laser desorption/ionization mass spectrometry (MALDI-MS) of membrane proteins and non-covalent complexes. *J. Mass Spectrom.*, **30**, 1462–14.

107 Cohen, L.H.R., Strupat, K., and Hillenkamp, F. (1997) Analysis of quaternary protein ensembles by matrix-assisted laser desorption/ionization mass spectrometry. *J. Am. Soc. Mass Spectrom.*, **8**, 1046–1052.

108 Song, F. (2007) A study of noncovalent protein complexes by matrix-assisted laser desorption/ionization. *J. Am. Soc. Mass Spectrom.*, **18**, 1286–1290.

109 Horneffer, V., Strupat, K., and Hillenkamp, F. (2006) Localization of noncovalent complexes in MALDI-preparations by CLSM. *J. Am. Soc. Mass Spectrom.*, **17**, 1599–1604.

110 Wortmann, A., Pimenova, T., Alves, S., and Zenobi, R. (2007) Investigation of the first shot phenomenon in MALDI mass spectrometry of protein complexes. *Analyst*, **132**, 199–207.

111 Terrier, P., Tortajada, J., Zin, G., and Buchmann, W. (2007) Noncovalent complexes between DNA and basic polypeptides or polyamines by MALDI-TOF. *J. Am. Soc. Mass Spectrom.*, **18**, 1977–1989.

112 Bich, C., Baer, S., Jecklin, M.C., and Zenobi, R. (2010) Probing the hydrophobic effect of noncovalent complexes by mass spectrometry. *J. Am. Soc. Mass Spectrom.*, **21**, 286–289.

113 Gruic-Sovulj, I., Lüdemann, H.C., Hillenkamp, F., Weygand-Duraseciv, I., Kucan, Z., and Peter-Katalinić, J. (1997) Detection of noncovalent tRNA aminoacyl-tRNA synthetase complexes by matrix-assisted laser desorption/ionization mass spectrometry. *J. Biol. Chem.*, **272**, 32084–32091.

114 Vogl, T., Roth, J., Hillenkamp, F., and Strupat, K. (1999) Calcium-induced non-covalently linked tetramers of MRP8 and MRP14 detected by ultraviolet matrix-assisted laser desorption/ionization mass spectrometry. *J. Am. Soc. Mass Spectrom.*, **10**, 1124–1130.

115 Kiselar, J.G. and Downard, K.M. (2000) Preservation and detection of specific antibody-peptide complexes by matrix-assisted laser desorption ionization mass spectrometry. *J. Am. Soc. Mass Spectrom.*, **11**, 746–750.

116 Woods, A.S. and Huestis, M.A. (2001) A study of peptide-peptide interaction by matrix-assisted laser desorption/ionization. *J. Am. Soc. Mass Spectrom.*, **12**, 88–96.

117 Woods, A.S., Koomen, J.M., Ruotolo, B.T., Gillig, K.J., Russel, D.H., Fuhrer, K., Gonin, M., Egan, T.F., and Schultz, J.A. (2002) A study of peptide-peptide interactions using MALDI ion mobility o-TOF and ESI mass spectrometry. *J. Am. Soc. Mass Spectrom.*, **13**, 166–169.

118 Luo, S.H., Li, Y.M., Qiang, W., Zhao, Y.F., Abe, H., Nemoto, T., Qin, X.R., and Nakanishi, H. (2004) Detection of

specific noncovalent interaction of peptide with DNA by MALDI-TOF. *J. Am. Soc. Mass Spectrom.*, **15**, 28–31.

119 Karas, M., Bahr, U., Ingendoh, A., and Hillenkamp, F. (1989) Laser desorption/ionization mass spectrometry of proteins of mass 100 000 to 250 000 Dalton. *Angew. Chem. Int. Ed. Engl.*, **28**, 760–761.

120 Hillenkamp, F., Karas, M., Beavis, R.C., and Chait, B.T. (1991) Matrix-assisted laser desorption ionization mass spectrometry of biopolymers. *Anal. Chem.*, **63**, 1193A–1203A.

121 Hillenkamp, F. (1998) *New Methods for the Study of Biomolecular Complexes; NATO ASI Series C: Mathematical and Physical Science 510*, Kluwer Academic Publishers, Dordrecht, The Netherlands, pp. 181–191.

122 Farmer, T.B. and Caprioli, R.M. (1998) Determination of protein-protein interactions by matrix-assisted laser desorption/ionization mass spectrometry. *J. Mass Spectrom.*, **33**, 697–704.

123 Zehl, M. and Allmaier, G. (2005) Instrumental parameters in MALDI-TOF mass spectrometric analysis of quaternary protein structures. *Anal. Chem.*, **77**, 103–110.

124 Zehl, M. and Allmaier, G. (2004) Ultraviolet matrix-assisted laser desorption/ionization time-of-flight mass spectrometry of intact hemoglobin complex from whole human blood. *Rapid Commun. Mass Spectrom.*, **18**, 1932–1938.

125 Lecchi, P. and Pannelle, L.K. (1995) The detection of intact double-stranded DNA by MALDI. *J. Am. Soc. Mass Spectrom.*, **6**, 972–975.

126 Kirpekar, F., Berkenkamp, S., and Hillenkamp, F. (1999) Detection of double-stranded DNA by IR- and UV-MALDI mass spectrometry. *Anal. Chem.*, **71**, 2334–2339.

127 Dybvik, A.I., Norberg, A.L., Schute, V., Soltwisch, J., Peter-Katalinić, J., Vårum, K.M., Eijsink, V.G.H., Dreisewerd, K., Mormann, M., and Sørlie, M. (2011) Analysis of noncovalent chitinase-chito-oligosaccharide complexes by infrared-matrix assisted laser desorption ionization and nanoelectrospray ionization mass spectrometry. *Anal. Chem.*, **83**, 4030–4036.

128 Bennett, K.L., Kussmann, M., Björk, P., Godzwon, M., Mikkelsen, M., Sørensen, P., and Roepstorff, P. (2000) Chemical cross-linking with thiol-cleavable reagents combined with differential mass spectrometric peptide mapping – a novel approach to assess intermolecular protein contacts. *Protein Sci.*, **9**, 1503–1518.

129 Gasilova, N. and Nazabal, A. (2012) Monitoring ligand modulation of protein-protein interactions by chemical cross-linking and high-mass MALDI mass spectrometry. *Methods Mol. Biol.*, **803**, 219–229.

130 Yanes, O., Villanueva, J., Querol, E., and Aviles, F.X. (2005) Functional screening of serine protease inhibitors in the medical leech *Hirudo medicinalis* monitored by intensity fading MALDI-TOF MS. *Mol. Cell. Proteomics*, **4**, 1602–1613.

131 Bich, C. and Zenobi, R. (2009) Mass spectrometry of large complexes. *Curr. Opin. Struct. Biol.*, **19**, 632–639.

132 Mädler, S., Erba, E.B., and Zenobi, R. (2013) MALDI-TOF mass spectrometry for studying noncovalent complexes of biomolecules. *Top. Curr. Chem.*, **331**, 1–36.

133 Ulmer, L., Mattay, J., Torres-Garcia, H.G., and Luftmann, H. (2000) Letter: the use of 2-[(2*E*)-3-(4-*tert*-butylphenyl)-2-methylprop-2-enylidene]malononitrile as a matrix for matrix-assisted laser desorption/ionization mass spectrometry. *Eur. J. Mass Spectrom.*, **6**, 49–52.

134 Sun, G., Yang, K., Zhao, Z., Guan, S., Han, X., and Gross, R.W. (2008) Matrix-assisted laser desorption/ionization time-of-flight mass spectrometric analysis of cellular glycerophospholipids enabled by multiplexed solvent dependent analyte matrix interactions. *Anal. Chem.*, **80**, 7576–7585.

135 Estrada, R. and Yappert, M.C. (2004) Alternative approaches for the detection of various phospholipid classes by matrix-assisted laser desorption/

ionization time-of-flight mass spectrometry. *J. Mass Spectrom.*, **39**, 412–422.

136 Przybylski, C., Gonnet, F., Bonnaffé, D., Hersant, Y., Lortat-Jacob, H., and Daniel, R. (2010) HABA-based ionic liquid matrices for UV-MALDI-MS analysis of heparin and heparan sulfate oligosaccharides. *Glycobiology*, **20**, 224–234.

137 Calvano, C.D., Carulli, S., and Palmisano, F. (2010) 1*H*-Pteridine-2,4-dione (lumazine): a new MALDI matrix for complex (phospho)lipid mixtures analysis. *Anal. Bioanal. Chem.*, **398**, 499–507.

138 Shroff, R. and Svatoš, A. (2009) Proton sponge: a novel and versatile MALDI matrix for the analysis of metabolites using mass spectrometry. *Anal. Chem.*, **81**, 7954–7959.

139 Qiao, H., Piyadasa, G., Spicer, V., and Ens, W. (2009) Analyte distribution in MALDI samples using MALDI imaging mass spectrometry. *Int. J. Mass Spectrom.*, **281**, 41–51.

140 Tholey, A. and Heinze, E. (2006) Ionic (liquid) matrices for matrix-assisted laser desorption/ionization mass spectrometry–applications and perspectives. *Anal. Bioanal. Chem.*, **386**, 24–37.

141 Szájli, E., Fehér, T., and Medzihradsky, K.F. (2008) Investigating the quantitative nature of MALDI-TOF MS. *Mol. Cell. Proteomics*, **7**, 2410–2418.

142 Weinberger, S.R., Boernsen, K.O., Finchy, J.W., Robertson, V., and Musselman, B.D. (1993) Proceedings, 41st Annual ASMS Conference on Mass Spectrometry and Allied Topics; San Francisco, CA, May 31–June 5, 1993, pp. 775a–775b.

143 Vorm, O., Roepstorff, P., and Mann, M. (1994) Improved resolution and very high sensitivity in MALDI TOF of matrix surfaces made by fast evaporation. *Anal. Chem.*, **66**, 3281–3287.

144 Dai, Y., Whittal, R.M., and Li, L. (1999) Two-layer sample preparation: a method for MALDI-MS analysis of complex peptide and protein mixtures. *Anal. Chem.*, **71**, 1087–1091.

145 Jaskolla, T.W., Karas, M., Roth, U., Steinert, K., Menzel, C., and Reihs, K. (2009) Comparison between vacuum sublimed matrices and conventional dried droplet preparation in MALDI-TOF mass spectrometry. *J. Am. Soc. Mass Spectrom.*, **20**, 1104–1114.

146 Röhl, H., Goethel, S., and Reihs, K. (2005) MPep MALDI chips for high-sensitivity and high-throughput peptide analysis by MALDI-TOF MS. *Nat. Methods*, **2**, 6. Application Note.

147 Schuerenberg, M., Luebbert, C., Eickhoff, H., Kalkum, M., Lehrach, H., and Nordhoff, E. (2000) Prestructured MALDI-MS sample supports. *Anal. Chem.*, **72**, 3436–3442.

148 Laugesen, S. and Roepstorff, P. (2003) Combination of two matrices results in improved performance of MALDI MS for peptide mass mapping and protein analysis. *J. Am. Soc. Mass Spectrom.*, **14**, 992–1002.

149 Karas, M., Ehring, H., Nordhoff, E., Stahl, B., Strupat, K., Hillenkamp, F., Grehl, M., and Krebs, B. (1993) Matrix-assisted laser desorption/ionization mass spectrometry with additives to 2,5-dihydroxybenzoic acid. *Org. Mass Spectrom.*, **28**, 1476–1481.

150 Zhu, Y.F., Chung, C.N., Taranenko, N.I., Allman, S.L., Martin, S.A., Haff, L., and Chen, C.H. (1996) The study of 2,3,4-trihydroxyacetophenone and 2,4,6-trihydroxyacetophenone as matrices for DNA detection in matrix-assisted laser desorption/ionization time-of-flight mass spectrometry. *Rapid Commun. Mass Spectrom.*, **10**, 383–388.

151 Pieles, U., Zürcher, W., Schär, M., and Moser, H.E. (1993) Matrix-assisted laser desorption ionization time-of-flight mass spectrometry: a powerful tool for the mass and sequence analysis of natural and modified oligonucleotides. *Nucleic Acids Res.*, **21**, 3191–3196.

152 Smirnov, I., Zhu, X., Taylor, T., Huang, Y., Ross, P., Papayanopoulos, I.A., Martin, S.A., and Pappin, D.J. (2004) Suppression of alpha-cyano-4-hydroxycinnamic acid matrix clusters and reduction of chemical noise in MALDI-TOF mass spectrometry. *Anal. Chem.*, **76**, 2958–2965.

153 Kjellström, S. and Jensen, O.N. (2004) Phosphoric acid as a matrix additive for

MALDI MS analysis of phosphopeptides and phosphoproteins. *Anal. Chem.*, **76**, 5109–5117.

154 Larsen, M.R., Thingholm, T.E., Jensen, O.N., Roepstorff, P., and Jorgensen, J.D. (2005) Highly selective enrichment of phosphorylated peptides from peptide mixtures using titanium dioxide microcolumns. *Mol. Cell. Proteomics*, **4**, 873–886.

155 Chen, C.T. and Chen, Y.-C. (2005) Fe_3O_4/TiO_2 core/shell nanoparticles as affinity probes for the analysis of phosphopeptides using TiO_2 surface-assisted laser desorption/ionization mass spectrometry. *Anal. Chem.*, **77**, 5912–5919.

156 Li, P., Zhang, D., and Guo, C. (2012) Serum biomarker screening for the diagnosis of early gastric cancer using SELDI-TOF-MS. *Mol. Med. Report.*, **5**, 1531–1535.

157 Zhang, K., Yuan, K., Wu, H., Li, Q., Wang, Y., Chen, S., Zhang, L., Gu, H., and Fu, R. (2012) Identification of potential markers related to neoadjuvant chemotherapy sensitivity of breast cancer by SELDI-TOF MS. *Appl. Biochem. Biotechnol.*, **166**, 753–763.

158 Armstrong, D.W., Zhang, L.K., He, L., and Gross, M.L. (2001) Ionic liquids as matrixes for matrix-assisted laser desorption/ionization mass spectrometry. *Anal. Chem.*, **73**, 3679–3686.

159 Sze, E.T.P., Chan, T.-W.D., and Wang, G. (1998) Formulation of matrix solutions for use in matrix-assisted laser desorption/ionization of biomolecules. *J. Am. Soc. Mass Spectrom.*, **9**, 166–174.

160 Towers, M.W., Mckendrick, J.E., and Cramer, R. (2010) Introduction of 4-chloro-α-cyanocinnamic acid liquid matrices for high sensitivity UV-MALDI MS. *J. Proteome Res.*, **9**, 1931–1940.

161 Meriaux, C., Franck, J., Wisztorski, M., Salzet, M., and Fournier, I. (2010) Liquid ionic matrixes for MALDI mass spectrometric imaging of lipids. *J. Proteomics*, **73**, 1204–1218.

162 Chan, K., Lanthier, P., Liu, X., Sandhu, J.K., Stanimirovic, D., and Li, J. (2009) MALDI mass spectrometry imaging of gangliosides in mouse brain using ionic liquid matrix. *Anal. Chim. Acta*, **639**, 57–61.

163 Soukop-Hein, R.J., Warnke, M.M., and Armstrong, D.W. (2009) Ionic liquids in analytical chemistry. *Annu. Rev. Anal. Chem.*, **2**, 145–168.

164 Trimpin, S., Keune, S., Rader, H.J., and Mullen, K. (2006) Solvent-free MALDI-MS: developmental improvements in the reliability and the potential of MALDI in the analysis of synthetic polymers and giant organic molecules. *J. Am. Soc. Mass Spectrom.*, **17**, 661–671.